# Dynamics and Control of Magnetic Manipulators

by

Sergei Lubensky

Submitted to the Department of Electrical Engineering and Computer Science
in partial fulfillment of the requirements for the degree of

Master of Engineering in Electrical Engineering and Computer Science

at the

MASSACHUSETTS INSTITUTE OF TECHNOLOGY

February 2002





Author .....
Department of Electrical Engineering and Computer Science
February 8, 2002

Certified by .....
Gill Pratt
MIT Affiliate
Thesis Supervisor

Accepted by .....
Arthur C. Smith
Chairman, Department Committee on Graduate Theses

# Dynamics and Control of Magnetic Manipulators

by

Sergei Lubensky

Submitted to the Department of Electrical Engineering and Computer Science
on February 8, 2002, in partial fulfillment of the
requirements for the degree of
Master of Engineering in Electrical Engineering and Computer Science

## Abstract

This thesis contains a survey and a general quantitative analysis of a family of devices based on magnetostatic interactions between a dipole magnet and a set of electromagnetic coils. Theoretical foundation is laid down for analyzing the dynamics of magnetic dipole in a non-uniform magnetic field, computing the field due to a current distribution in a set of solenoidal coils, and deriving optimal control strategies based on the geometry of the field sources, the dynamics constraints of the problem, and on the considerations of overall power efficiency. The issues of technological feasibility and fundamental limitations of the proposed mechanisms for magnetic manipulation are addressed on the basis of theoretical findings presented in this thesis and elsewhere in the literature. Major technological challenges are identified and recommendations are made for future research and developments in the area.

Thesis Supervisor: Gill Pratt
Title: MIT Affiliate

# Acknowledgments

This has been a long and arduous trip for me – much longer than anybody could reasonably expect. Looking back now, I can say with certainty that I would not have gotten to this point if it was not for the generous help and support of the many friends and mentors that I was fortunate enough to have around. And without them, I would not have had all those memorable experiences that I can take away with me now. To all those who found the strength to believe in me when I could not; to all who have helped so abundantly and who have inspired me, despite all odds, to stay on this path; to all of them goes my deepest gratitude and respect for their infinite patience and kindness. Thank you all so much!

My special thanks go to Prof. Gill Pratt – a great scientist and a wonderful person! To my friends and colleagues, Boris Kozinsky and Vadim Khayms – I could not have done it without you guys! To all the people at PSFC who have made it a home for me. To my Dutch friends and roommates, Pieter Thomasson and Casper Doppen, who have permanently stricken the word "dull" (or normal?) from my vocabulary. To the "Walking Chinese," who unknowingly came to epitomize "The Great Cycle of Change" and the sheer futility of being in one place for more than ten minutes.

To Anne Hunter – the best program administrator there has ever been -- a beacon of hope and a source of joy to great many of us in this department. If it was not for her inexhaustible patience and empathy, I would have become an alumnus much sooner than I intended to.

To my family, who have always encouraged and supported me through everything, in spite of my earnest efforts to dissuade them from doing so.

To my best friend, Alex Bazhanov, who has single-handedly pulled me through what must have been the most difficult period in my life and in my work, for that matter.

My most profound affection goes to my longtime friend and true love, Tanya Shilova. If there is one single person who deserves the credit for this deed, it is she; for no one knows how much love and energy and caring she has invested in this venture without the slightest hope of success. Tanya, I admire your grace and courage and dedicate this work to you. Thank you so much for being a part of my life!

# Table of Contents

# List of Figures



# List of Tables

# Chapter 1

# Introduction

Many of us have played, as children, with small magnets and acquired intuition about some basic facts, such as that each magnet has two ends ("poles") and any two magnets attract when facing each other in one orientation and repel in the other. We also learned about the compass needle and its propensity to point in one particular global direction: that of the magnetic field of the earth. Furthermore, we discovered how magnets move about in space when their neighbors are displaced and how some nonmagnetic objects start acting like magnets in the presence of one. All these phenomena are manifestations of magnetostatics, a field that has been studied for many centuries, long before magnetism was related to electricity via Maxwell's equations, before its nature was elucidated with the aid of the special theory of relativity and before its origins in matter were described with quantum mechanics.

The basic empirical principle of magnetostatics is very tangible and relevant to our everyday experience: it is called "action at a distance." One magnet exerts a torque and a force on another magnet in its vicinity; the torque acts to align the two magnets in a parallel orientation and the force acts to pull them together. Magnetic forces, thus produced, are arguably, the most convenient means of manipulating electrically neutral

objects at a distance: they directly involve no friction and require no medium for their transmission, *e.g.*, no physical connection between the interacting components.

## 1.1 Overview

The idea of magnetic manipulation has been utilized in various forms in a host of important applications, most notable of which are:

1) Magnetomechanical conversion machines (motors and generators)
2) Pulsed eclectromagnetic power production (dynamo machines)
3) Magnetic bearings and suspensions (including atomic traps and wind tunnels)
4) Decceleration of an electric conductor crossing magnetic field (brakes)
5) Levitation of magnets over a magnetic or conducting track (MAGLEV trains)

All of these applications make use of the same physical idea, but none pursue it directly. The idea consists of positioning and moving a magnet in space by adjusting the field sources, which effectively serve as actuators. It corresponds closely with the basic intuition that we gain from playing with toy magnets. However, in spite of the simplicity of this idea, there are surprisingly few systems that are specifically designed to embody it. Of the applications listed above, those from the third and fifth categories can, in principle, serve the purpose. However, the former go only part of the way because they always maintain a magnet in the same place and the latter do not fit the description because the magnet that is being moved comprises an integral part of the actuating

system. The subject matter of this thesis is concerned with a class of systems, collectively termed *magnetic manipulators*, whose sole purpose is to produce a specified motion of a dipole magnet in a contained region of space, where the dimensions of the dipole are much smaller than those of the containment region. The objective of the present study is to illuminate their principles of operation and outline their capabilities and limitations, in the most general setting possible.

## 1.2 Background

### 1.2.1 Problem Definition

The fundamental principle of magnetic manipulators is that magnetic fields and their gradients, typically generated by large electromagnetic coils, can be used to produce torques and forces on a small permanent magnet in order to guide it along the desired trajectory inside the operating volume. The design of such systems ultimately depends on the intended regime of motion, the operating constraints, the specified performance criteria, and the geometry of the problem. Accordingly, they can be broadly categorized into magnetic levitation, rotation, and propulsion systems, depending on the type of motion; one-, two-, and three-dimensional, small- and large-gap, depending on the geometry; and, static (DC), quasi-static (low frequency), and dynamic (AC) depending on the actuator control bandwidth.

This list is by no means exhaustive, but even so, it spans a whole gamut of different dynamical behaviors and requirements. Examples of levitation systems include magnetic suspension and balance systems (MSBS) used to measure aerodynamic forces and torques on model planes suspended in wind tunnels and frictionless magnetic bearings used in ultracentrifuges and in various diagnostic systems. The former is inherently a large-gap quasi-static 3-D application, while the latter is typically designed for small gaps and 2-D AC fields. Homopolar generator (dynamo) is an example of a static small-gap two-dimensional magnetomechanical system where current pulses are produced on the surface of a metallic disc rotated inside the bore of a magnet. Exactly the opposite effect is achieved in electric motors, where magnetic field is rotated in 2-D to produce rotational motion of the shaft. Examples of translational 1-D systems include magnetic braking, dipole suspension, and particle acceleration systems. High-speed ground transportation of magnetically levitated vehicles (MAGLEV) exemplifies a 2-D translational system that exists in both AC and DC configurations. The common trend is for AC systems to be small-gap and usually confined to rotation in a plane while translational systems are mostly DC and typically low-dimensional.

### 1.2.2 Technical Challenges

The most rare beast in this menagerie of magnetic systems is a large-gap configuration where a time-varying field is used to produce translational motion in several dimensions. This rarity can be attributed to some inherent problems in energetics and controllability of such systems. Transmitting forces across large gaps typically requires powerful field

sources, and the intrinsic properties of the magnetic field, dictated by the Maxwell's equations, further complicate the matters by precluding the possibility of concentrating useful energy in a localized region of space.[1] Most of the existing sources of strong magnetic fields are DC because the time-varying systems dissipate a lot of energy in the form of heat. The use of superconducting materials in the construction of electromagnets alleviates the problem to some extent, because of the tremendous reduction in the amount of resistive dissipation.

However, a host of new problems arises because the superconductors must be kept at extremely low temperatures ($<12°$K for types I&II, $\sim 75°$K for HTS) to maintain their superconducting state and the heat produced as a result of inductive AC losses and eddy-currents must be removed faster than it is generated. The capacity of the cryogenic cooling systems thus determines the maximum allowable rate at which the fields can be changed, and this limitation is typically stringent enough to seriously hinder the development of any practical superconducting AC system. However, recent advances in the superconducting technology have improved the situation considerably, and the emerging generation of large gap superconducting AC systems is holding a great promise for many potential areas of applications, such as medicine, manifacturing, and aviation.

Alongside the problems with energetics, another set of issues arises in the area of control of such systems. The open-loop dynamics associated with magnetic fields and forces is

[1] Potential energy of the magnet is proportional to the strength of the magnetic field. In the absence of time-varying currents inside the operating space, the field must be a solution to the Laplace equation, $\Delta\mathbf{B} = -\nabla\times(\nabla\times\mathbf{B}) = 0$, and thus a harmonic function. As such, it cannot have highly localized spatial gradients. Thus, the field and the energy must remaing large in the vicinity of their maxima.

inherently non-linear and unstable. In fact, it is impossible even to achieve stability at a single point without the use of a feedback control or some non-magnetic damping forces. The reason is another consequence of Maxwell's equations, as conveyed in the celebrated Earnshaw's theorem.[2] Active suspension systems, such as MSBS, are optimized for using feedback position control optimized for a single spatial location of equilibrium. However, for a translational system, the magnet is allowed to move inside the operating volume and adequate control of the forces and torques must be achieved at all the points along its trajectory. For large volumes and dimensions higher than one, this consideration complicates the problem tremendously through the "curse of dimensionality" – the term coined by Bellman for this kind of problems in optimal control. As a consequence, there are very few magnetic systems, even resistive ones with small gaps, that are capable of producing controllable motion along any trajectory within a contained volume of space.

### 1.2.3 The Roadmap

In order to investigate the issues presented above and to assess their solvability in a systematic way, we will focus our attention on the subset of such systems consisting of two-dimensional quasi-static large-gap manipulators. The first qualifier suggests that the motion of a magnet is either restricted to a surface or can be approximated as planar for any sufficiently long period of time. The second implies that characteristics of the field

---

[2] The gradient of magnetic force is zero $\nabla \cdot \mathbf{F} = \nabla \cdot (\mathbf{p} \cdot \nabla)\mathbf{B} = -\nabla \cdot \nabla \times \{\nabla \times (\mathbf{p} \times \mathbf{B})\} = 0$ and the same is true for the torque $\nabla \cdot \mathbf{T} = \nabla \cdot (\mathbf{p} \times \mathbf{B}) = \mathbf{B} \cdot (\nabla \times \mathbf{p}) - \mathbf{p} \cdot (\nabla \times \mathbf{B}) = 0 - 0 = 0$. If an equilibrium stable, the forces and torques must point toward it on the surface of some surrounding sphere. However, by Gauss' theorem, $\oiint \mathbf{F} \cdot d\mathbf{s} = \iiint \nabla \cdot \mathbf{F}\, dV = \iiint 0\, dV = 0$ and likewise for the torque. There will always be instability to some lateral displacement or rotation of the body about any position of equilibrium.

sources (such as currents in the coils) are adjusted slowly enough that their controls can be considered as step inputs with smooth ramping between the constant levels. Finally, the third qualifier can be interpreted as the requirement that the distance between the manipulated object and the source of the field must be at least an order of magnitude larger than the size of the object itself. The reasons for selecting this particular category of magnetic manipulators are as follows.

Planar motion is chosen for simplicity of vizualization and computation: 3-D is too complex, while 1-D does not demonstrate some essential aspects of motion, such as "skidding" (moving sideways). However, some approximate analytical calculations will be carried out in 1-D, where appropriate, while certain important issues, such as those concerning static magnetic traps, will be discussed in the context of a 3-D problem because they do not manifest themselves in the lower dimensions. The choice of the quasi-static regime of motion represents a tradeoff between the ability to direct the magnet along any desired trajectory and the constraints imposed on the actuators and sensors by a high-bandwidth control. Furthermore, this regime represents well the dynamics of motion in a damping medium and the control dynamics of a human operator. Finally, the restriction of the frequency of inputs to a low range ($\sim 1-10$ Hz) makes their calculation more tractable and facilitates both the design and analysis of the control algorithms and their real-time implementation on a micro-controller.

Accepting the practical necessity of the above limitations, we will otherwise consider the problem of propulsion in the most general terms. No *a priori* assumption will be made

about the geometry of the problem; thus, all directions of motion will be considered on equal footing and the dynamic requirements will be the same for all spatial positions and orientations of the magnet. The angular and radial symmetry of the problem, together with the 2-D restriction, suggests a circular shape for the operating volume. In order to make possible a wide repertoire of motion trajectories, the size of the operating volume has to be sufficiently larger than that of the magnet itself; hence, the large-gap criterion: $r/l > 10:1$, where $r$ is the radius of the circle and $l$ is the length of the magnet.

Likewise, no specific assumptions will be made about the torques and forces exerted on the magnet, other than that their magnitudes and rates of change will be limited by some maximum achievable values. Although these limiting values will have to be chosen somewhat arbitrarily, their relation to the capacity of some real systems of actuators and, in particular, their scaling properties with the inputs will be discussed in some detail. Notwithstanding the generality of approach, certain performance measures corresponding to some specific practical considerations, will be applied in the analysis and optimization of different dynamical scenarios, so that some configurations of forces and torques will be deemed more desirable than others. For example, the degree of allignment of the magnet with its direction of motion will be accounted for in such analysis and the issues of power efficiency will be investigated in the context of a particular system of actuators.

For the purposes of this analysis, the system of actuators will be modeled by a set of circular electromagnetic coils, all centered on the plane of motion of the magnet, and oriented perpendicular to it. Each coil will be driven by an independently controlled

power supply, represented as a voltage source in series with some finite resistance. The resistance of the coils themselves will be neglected and only their inductive properties will be considered. Some of the calculations will account for the finite cross-section of the coils while others will treat them as single windings. In either case, the thickness or cross-sectional geometry of the coils will be considered fixed; however, the radius and orientation of each coil, as well as the coordinates of its center on the plane of motion will be adjustable for optimization purposes, subject only to the constraint that the coils do not overlap in space and do not intersect the operating volume.

For the purposes of dynamic analysis, such a model should prove general enough to encompass not only a variety of resistive and superconducting electromagnets, but also some permanent magnet assemblies and combinations thereof. More comprehensive models that include, for instance, the ramp-rate limitations of superconductors and the limits on the capacity of the power supplies, will be in order when the dynamics, constraints, and performance criteria of a particular system are specified in more detail. The present analysis should be applicable as a starting point in the design and evaluation of such a system.

# Chapter 2

# Dynamics of Magnetic Dipole

## 2.1 Dipole Model of a Magnet

If the dimensions of the manipulated permanent magnet are very small compared to the size of the coils, the former can be idealized as a point dipole, whose magnetic properties can be summarized in a single vector, the total magnetic moment, **p**. Its direction is the same as the north-pole orientation of an equivalent bar magnet and its magnitude is proportional to the magnet's strength and volume. This vector represents the magnetic field generated by the magnet itself, due to its intrinsic magnetic property, called magnetization, **M**, and defined as the magnetic moment density,

$$\mathbf{p} = \int \mathbf{M}_V \cdot dV \,. \tag{2.1}$$

Magnetic properties of materials, described by their magnetization, depend on two main atomic effects, which can give rise to large local magnetic fields: the orbital motion of electrons around the nucleus and the intrinsic spin of the electrons. In the presence of an ambient magnetic field, **H**, these effects manifest themselves differently and produce a

range of magnetic behaviors in different materials. The relationship between the magnetic field, $\mathbf{H}$, and magnetization, $\mathbf{M}$, is captured by the material property called *susceptibility*, $\chi_m$, defined as

$$\mathbf{M} = \chi_m(\mathbf{H}) * \mathbf{H} \ . \tag{2.2}$$

Magnetic susceptibility varies widely for different materials and, in general, depends in a complicated way on both the present field, $\mathbf{H}(t)$, and on its past values $\{\mathbf{H}(\tau) \mid \tau < t\}$. For heuristic purposes, materials are broadly categorized as *diamagnetic*, *paramagnetic*, and *ferromagnetic*. Diamagnetic materials have negative susceptibility and tend to push themselves toward the regions of lower magnetic field. Their magnetization is usually small compared to the strength of the external field. This group includes water, organic compounds, and some metals, such as bismuth, copper and silver. Paramagnetic materials have permanent magnetic moments that tend to align themselves in the direction of the external field. The total magnetic moment points in the field direction and varies nearly linearly with the field strength, yielding a relatively small positive constant susceptibility coefficient. This group includes several gases, such as oxygen, and light metals, such as aluminum and sodium. Unlike diamagnetics, paramagnetic substances are strong field seekers – they tend to push themselves in the direction of the field gradient. For the purposes of magnetic manipulation, the susceptibility of both diamagnetic and paramagnetic materials is too small ($\sim 10^{-5}$) to produce forces and energy densities of sufficient magnitude for most practical applications.

By contrast, ferromagnetic materials exhibit exceptionally strong magnetization $(10^4 - 10^6)$ and several other important properties which make them the primary choice for the role of magnetically manipulated objects. Ferromagnetics are characterized by microscopic domains $(10^{10} - 10^{15}\text{atoms})$, where all magnetic moments are fully aligned, due to certain quantum-mechanical properties of their crystalline structure. The total magnetization of the material is a vector sum of each domain's magnetization. When the orientation of the magnetic moment of each domain is at random, there is no total magnetization in the bulk material. However, with the application of external magnetic field, all domains gradually align in the field direction.

Unlike the paramagnetic interactions, this effect is emphatically non-linear and depends strongly on the structure of the domains and the evolution of the fields. When a magnetic field is applied, the domains change and their walls displace correspondingly across the crystal until they reach an imperfection or a grain boundary in the lattice. These imperfections introduce a resistance to falling back to the initial state when the external field is removed. Thus, some induced magnetization, called *magnetic remanence* $B_r$, persists in the magnet in the absence of the applied field. Furthermore, if the field is then reversed, it has to reach an appreciable value, called *coercivity* $H_c$, in order to cancel remaining induction in the magnet. In general, magnetization and relaxation take place along different curves in the *B-H* plane: the phenomenon known as *hysteresis.*

The existence of persistent memory in a ferromagnet and the way in which microscopic imperfections of the lattice influence the magnetization process on a macroscopic scale,

suggest an interesting possibility of controlling the global magnetic properties of a dipole and hence, its potential energy in the presence of a large but uniform and constant magnetic field, through local alterations of its mechanical or chemical structure. This would be akin to the operation of a MOSFET transistor, where small voltage applied at the gate terminal can control large currents flowing between the drain and the source. In this case, the controlling variable may be a microscopic difference in chemical potential, mechanical stress, or local temperature gradient, and the controlled variable would be the potential energy of the dipole in a large ambient magnetic field. By exploiting such possibility, one can, in principle, avoid the problem of large changing magnetic fields by creating the same effect at the local level of the dipole. Furthermore, in this scheme several dipoles can be controlled independently in the same field. However, for the time being, we shall consider the properties of the dipole to be constant in space and time and the dipole dynamics to be determined exclusively by the magnetic field and its spatial and temporal derivatives.

## 2.2 Dipole Dynamics

Magnetic forces and torques exerted on the magnet can be derived most easily on the basis of virtual work formalism. As a starting point, we consider the expression for the potential energy of a dipole in the presence of magnetic field,

$$U = -\mathbf{p} \cdot \mathbf{B}. \tag{2.3}$$

The energy, in general, depends on several independent parameters, $x_i$, so that the energy increment can be expressed as

$$\delta U = \sum_i \frac{\partial U}{\partial x_i} \delta x_i \,. \tag{2.4}$$

By the principle of conservation of energy, this increment corresponds to the work done by the generalized force, $\mathbf{F}$, and related to the change of parameters $x_i$ via

$$-\delta U = \delta W = \sum_i F_{x_i} \delta x_i \,. \tag{2.5}$$

Therefore, the force components can be expressed as

$$F_{x_i} = -\frac{\partial U}{\partial x_i} \,. \tag{2.6}$$

When the parameters are chosen to be the cartesian spatial coordinates, $\{x, y, z\}$, the force vector becomes

$$\begin{aligned} &\mathbf{F} = -\nabla U = \nabla(\mathbf{p} \cdot \mathbf{B}) = \\ &\sum_{s=\{x,y,z\}} \left[ \mathbf{p} \cdot \frac{\partial \mathbf{B}}{\partial s} \right] \hat{\mathbf{s}} = \left[ p_x \frac{\partial B_x}{\partial x} + p_y \frac{\partial B_y}{\partial x} + p_z \frac{\partial B_z}{\partial x} \right] \mathbf{e}_x + [\cdots] \mathbf{e}_y + [\cdots] \mathbf{e}_z \end{aligned} \tag{2.7}$$

In the most general case, the dipole moment, $\mathbf{p}$, is not fixed in space and can assume an arbitrary angle $\theta$ with the field vector, $\mathbf{B}$. The dipole differential can then be defined as

$$d\mathbf{p} = d\theta \times \mathbf{p} \tag{2.8}$$

and the corresponding energy variation can be expressed as

$$dU = -\mathbf{p} \cdot d\mathbf{B} - d\mathbf{p} \cdot \mathbf{B}, \tag{2.9}$$

where the first term corresponds to the translational motion in the field gradient, while the second term corresponds to the rotational motion and leads to the following definition of the torque

$$\mathbf{T} = \mathbf{p} \times \mathbf{B} \,. \tag{2.10}$$

Indeed,

$$d\mathbf{p}\cdot\mathbf{B}=(d\theta\times\mathbf{p})\cdot\mathbf{B}=d\theta\cdot(\mathbf{p}\times\mathbf{B})=d\theta\cdot\mathbf{T}. \tag{2.11}$$

Thus, a dipole in a magnetic field tends to rotate to align itself with the direction of the field, thereby acquiring its minimal potential energy; it is then accelerated most effectively by the field gradient.

## 2.3 Translation vs. Rotation

A natural question at this time would be whether rotational motion precedes translation entirely and, if not, to what extent is the dipole moment aligned with the field when it begins to move forward. To answer this question definitively, we need to specify the external dynamics: the non-magnetic forces and torques acting on the dipole. For example, if the magnet is constrained to point in a certain direction, it need not align itself with the field and, vice versa, if the drag on the magnet is much larger than the rotational damping, there will always be perfect alignment before any translational motion ensues. These issues are not that far-fetched and deserve a serious consideration in the context of a real problem. However, for the present purposes, we will ignore all external dynamics and analyze unconstrained motion of a dipole in the absence of any damping medium.

Assume the following parameters for the problem:

- The dipole is a circular cylinder, magnetized along its central axis, with density $\rho$, length $l$, radius $r$, and magnetization $M$.

- Derivative properties of the dipole are: its mass $m = \rho \cdot V$, magnetic moment $p = M \cdot V$, and the moment of inertia $I = \frac{1}{3} m \left( l/2 \right)^2 = \frac{m \cdot l^2}{12}$.
- The magnitude of the magnetic field at a point **s** is denoted by $B = \left\| \mathbf{B}(\mathbf{s}) \right\|$ and the magnitudes of the associated force and torque are $F$ and $T$, respectively.
- The center of mass of the dipole is located at point **s** and its angle with the field vector **B** is $\varphi$. In unit time, the dipole is translated in space through the distance of $\delta s$ and rotated through the arc of length $\lambda = \frac{l}{2} \cdot \delta\varphi$.
- To answer the original question, we define a dimensionless parameter

$$\gamma = \frac{\delta s}{\lambda} = \frac{ds}{d\varphi} \cdot \frac{2}{l}. \tag{2.12}$$

If

$\gamma \ll 1 \Rightarrow$ rotation happens first
$\gamma \gg 1 \Rightarrow$ translation happens first
$\gamma \approx 1 \Rightarrow$ rotation and translation occur on the same time scale.

In order to discuss the dynamics, we express $\gamma$ in terms of the second derivatives in time:

$$\frac{ds}{d\varphi} = \frac{\dot{s}}{\dot{\varphi}} \simeq \frac{d^2 s}{dt^2} \delta t \Big/ \frac{d^2 \varphi}{dt^2} \delta t = \frac{\ddot{s}}{\ddot{\varphi}}, \tag{2.13}$$

$$\gamma = \frac{\ddot{s}}{\ddot{\varphi}} \cdot \frac{2}{l}. \tag{2.14}$$

For translational motion,

$$\ddot{s} = \|\ddot{\mathbf{s}}\| = \frac{\|\mathbf{F}\|}{m} = \frac{\|\nabla(\mathbf{m}\cdot\mathbf{B})\|}{\rho\cdot V} = \frac{\|\nabla(M\cdot\cancel{V}\cdot B\cdot\cos\varphi)\|}{\rho\cdot\cancel{V}}$$
$$= \frac{M\cdot\cos\varphi}{\rho}\|\nabla B\| \tag{2.15}$$

For rotational motion,

$$\ddot{\varphi} = \frac{T}{I} = \frac{p\cdot B\cdot\sin\varphi}{m\cdot l^2/12} = \frac{M\cdot\cancel{V}\cdot B\cdot\sin\varphi}{\rho\cdot\cancel{V}\cdot l^2/12}$$
$$= \frac{12M\cdot\sin\varphi}{\rho\cdot l^2}B \tag{2.16}$$

Thus,

$$\gamma = \frac{\cancel{2}}{\cancel{1}}\cdot\frac{\cancel{M}\cos\varphi}{\cancel{\rho}}\cdot\|\nabla B\|\cdot\frac{l^{\cancel{2}}}{\cancel{2}\cdot 6}\cdot\frac{\cancel{\rho}}{\cancel{M}\sin\varphi}\cdot\frac{1}{B}$$
$$= \frac{l}{6}\cot\varphi\cdot\frac{\|\nabla B\|}{B} \tag{2.17}$$

In the spirit of dimensional analysis, we define the critical length, $D$, via

$$\|\nabla B\| \sim B/D. \tag{2.18}$$

Then,

$$\gamma \sim \left(l/D\right)\cot\varphi. \tag{2.19}$$

Since we defined a large-gap system is defined by

$$l/D < \frac{1}{10}, \tag{2.20}$$

translation and rotation will occur on the same time scale if

$$\cot\varphi = 10 \quad\Rightarrow\quad \varphi \approx \varphi^* = \cot^{-1}10 \simeq \frac{\pi}{30} = 6^\circ \tag{2.21}$$

Therefore, in the most general setting, we can assume that the magnet is aligned with the field to within $\sim 6^\circ$ before the translational motion becomes significant. Later on, when

we compute the expression for the magnetic field as a function of spatial coordinates, this assumption will be verified and refined.

# Chapter 3

# Magnetic Field of a Coil

Throughout this work, we will make use of four different expression for the magnetic field of a circular coil. First, we will consider a single circular winding and compute the field produced along its central axis. This consideration will yield a very simple one-dimensional analytical expression that can be used for preliminary optimization and first-order analysis of the problem. Then, an exact analytical expression for the 2-D field of the winding will be presented. The intrinsic symmetry of the problem will afford a simple extension of this result to the three-dimensional space. This expression will be used as a computational tool for dynamic simulations; its analytical form should prove advantageous in facilitating the real-time calculations in MATLAB and Simulink.

Next, we will model the field of a more realistic coil with finite cross-section with the aid of SOLDESIGN: a third-party finite-element code widely accepted in the scientific community and calibrated against experimental data. The output of the program will be tabulated on a spatial grid and interpolated for future computations. The resulting table will form the basis for the most accurate of our representations of a hypothetical but realistic system of electromagnetic actuators. In particular, it will serve as the input to

our optimization code designed to evaluate the capabilities and limitations of such a system. Finally, the tabulated data will be approximated with a family of simple analytical functions in order to facilitate a formal analysis of the dynamics of the system and aid in formulation of the optimal control strategies by enabling the use of classical tools of the Variational Calculus together with the computational techniques in Dynamic Programming.

## 3.1 Axial Field of a Circular Winding

The usual starting point for calculating magnetic fields produced by current-carrying conductors is the law of Biot-Savart:

$$\mathbf{B}(\mathbf{s}) = \frac{\mu_0}{4\pi} \oint \frac{I \cdot d\mathbf{l} \times \hat{\mathbf{r}}}{r^2}, \tag{3.1}$$

and its differential form

$$d\mathbf{B} = \frac{\mu_0}{4\pi} \frac{I \cdot d\mathbf{l} \times \mathbf{r}}{r^3}, \tag{3.2}$$

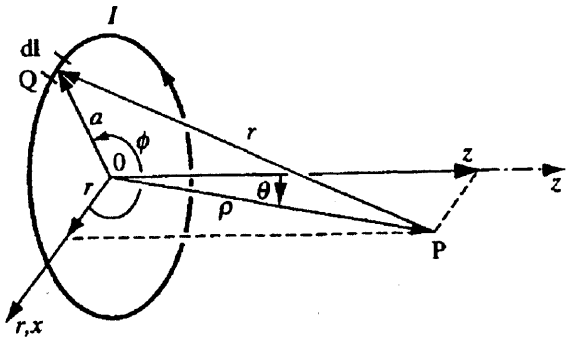


**Fig. 3.1 Current Loop and Coordinate System**[3]

where

$\mu_0 = 4\pi \cdot 10^{-7}\ {}^{H}/_{m}$ is the permeability of free space

$I$ – is the total current flowing in the conductor

$d\mathbf{l}$ – is the vector whose magnitude is the length of infinitesimal current carrying segment and whose direction is that of the current

$\mathbf{r}$ – is the vector from the field point to the infinitesimal conductor element

For a circular loop of wire of radius $a$ carrying current $I$, a small segment $dl$ produces magnetic field of magnitude

$$dB = \frac{\mu_0}{4\pi}\frac{I \cdot dl}{z^2 + a^2}. \tag{3.3}$$

The direction of this magnetic field is perpendicular to the line connecting $dl$ and the point on the axis. The components parallel to the line cancel due to the symmetry of the problem. Integrating the perpendicular components around the circle, we obtain

$$B = \oint dB_z = \oint \frac{\mu_0 I}{4\pi}\frac{\sin\theta \cdot dl}{z^2 + a^2} = \frac{\mu_0 I}{4\pi}\frac{a/\sqrt{z^2 + a^2}}{z^2 + a^2}\oint dl$$

[3] Reprinted from [1], p.92

$$= \frac{\mu_0 I}{4\pi} \frac{a}{\left(z^2 + a^2\right)^{3/2}} 2\pi a = \frac{\mu_0 I a^2}{2\left(z^2 + a^2\right)^{3/2}} \tag{3.4}$$

We can now proceed to compute the derivatives of this field:

$$\|\nabla B\| = \left|\frac{\partial B}{\partial z}\right| \propto \left|\frac{-3a^2 z}{\left(a^2 + z^2\right)^{5/2}}\right| = \frac{3/2\,\mu_0 I a^2 z}{\left(a^2 + z^2\right)^{5/2}} \tag{3.5}$$

$$\frac{\partial B}{\partial a} \propto \frac{2a}{\left(a^2 + z^2\right)^{3/2}} - \frac{3a^3}{\left(a^2 + z^2\right)^{5/2}} = -\frac{\mu_0 I a}{2} \frac{\left(a^2 - 2z^2\right)}{\left(a^2 + z^2\right)^{5/2}} \tag{3.6}$$

$$\frac{\partial^2 B}{\partial z \partial a} \propto \frac{4az}{\left(a^2 + z^2\right)^{5/2}} + \frac{5az\left(a^2 - 2z^2\right)}{\left(a^2 + z^2\right)^{7/2}} = 3/2\,\mu_0 I a z \frac{\left(3a^2 - 2z^2\right)}{\left(a^2 + z^2\right)^{7/2}} \tag{3.7}$$

$$\begin{aligned} \frac{\partial}{\partial a}\left(\frac{\partial^2 B}{\partial z^2}\right) &\propto 3a \frac{\left(3a^2 - 2z^2\right)}{\left(a^2 + z^2\right)^{7/2}} - \frac{12az^2}{\left(a^2 + z^2\right)^{7/2}} - 21az^2 \frac{\left(3a^2 - 2z^2\right)}{\left(a^2 + z^2\right)^{9/2}} \\ &= 3/2\,\mu_0 I a \frac{\left(3a^4 - 24a^2 z^2 + 8z^4\right)}{\left(a^2 + z^2\right)^{9/2}} \end{aligned} \tag{3.8}$$

## 3.2 Rotation vs. Translation Revisited

This would be a convenient point to revive the following questions regarding the relative time scale for rotational and translational motions of a magnetic dipole:

- What is the critical length in this problem, as defined in Eqn. 2.18 ?
- How should we modify our analysis from section 2.3 ?
- For a coil of given radius, where on its axis is the difference between rotational and translational dynamics most pronounced ?

The answer to the first question is,

$$D = \frac{B}{\left| \partial B / \partial z \right|} = \frac{a^2 + z^2}{3|z|}. \tag{3.9}$$

Computing the spatial derivative and setting it to zero:

$$\frac{\partial D}{\partial z} = \frac{1}{3}\operatorname{sgn} z \cdot (2 - \frac{a^2 + z^2}{z^2}) = \pm \frac{z^2 - a^2}{3z^2} \equiv 0, \tag{3.10}$$

we discover that $D$ assumes one extremum value at $z = a$. Since

$$\frac{\partial^2 D}{\partial z^2} = \operatorname{sgn} z \cdot \frac{2a^2}{3z^3} = \frac{2a^2}{3|z^3|} > 0 \quad \forall z, \tag{3.11}$$

it is a global minimum. Therefore,

$$D \geq \frac{2a^2}{3a} = \frac{2}{3}a. \tag{3.12}$$

and

$$\gamma \leq \frac{l}{6}\cot\varphi \cdot \frac{3}{2a} = \frac{l}{4a}\cot\varphi. \tag{3.13}$$

Once again, assuming that $l/a < \frac{1}{10}$, we obtain that the rotation is at least an order of magnitude faster than translation for all angles

$$\varphi \in \left[\frac{\pi}{10}, \frac{9\pi}{10}\right], \tag{3.14}$$

which applies to a smaller part of the circle than Eqn. 2.21, but also makes a stronger statement. In either case, the qualitative result is the same: unless the magnet is aligned fairly closely with the field (parallel or anti-parallel), rotation will dominate translation. The above analysis shows that in the worst case scenario, $z = a$, the angular sector where the time scales are comparable will be less than $1/10$ of the full circle.

## 3.3 Coil Size Optimization

Based on the expressions for the field and its derivatives, we can now evaluate where on the axis, the coil is most effective in creating a field or field gradient that would control the dynamics of a dipole placed at that location, via equations 2.7 and 2.10. In order to generalize our results for coils of arbitrary radii, we begin by expressing the field and its derivatives in terms of the dimensionless scaling factor, $\xi = z/a$.

$$B(\xi,a) = \frac{\mu_0 I}{2}\frac{1}{a\left(\xi^2+1\right)^{3/2}} \tag{3.15}$$

$$\left\|\nabla B(\xi,a)\right\| = \frac{3\mu_0 I}{2}\frac{\xi}{a^2\left(\xi^2+1\right)^{5/2}} \tag{3.16}$$

$$B_a(\xi,a) = \mu_0 I\frac{\left(\xi^2-1/2\right)}{a^2\left(\xi^2+1\right)^{5/2}} \tag{3.17}$$

$$B_{az}(\xi,a) = -3\mu_0 I\frac{\xi\left(\xi^2-3/2\right)}{a^3\left(\xi^2+1\right)^{7/2}} \tag{3.18}$$

$$\frac{\partial}{\partial a}\left[B_{zz}(\xi,a)\right] = 3/2\,\mu_0 I\frac{\left(3-24\xi^2+8\xi^4\right)}{a^4\left(\xi^2+1\right)^{9/2}} \tag{3.19}$$

The expressions above show that for a given scaling factor, $\xi$, the magnitude of the axial field varies inversely with the coil radius; that is, when viewed on the same scale, smaller coils produce larger fields. This fact is somewhat bewildering because one's intuition would suggest that the physics remains the same when the coils are scaled the same way. The phenomenon can be explained as follows. A field in space exists due to the motion of charged particles, *e.g.* electrons inside a circular wire. The current in the wire is

proportional to the linear velocity of the electrons passing through its cross-section at any given time. However, to an observer sitting at the point where the field is measured, the current appears proportional to the number of electrons passing through the cross-section in unit time; hence – to the angular velocity of the electrons. When linear velocity is fixed, the angular velocity is inversely proportional to the radius of the wire, and so is the field magnitude. For the same reason, the $n_{th}$ order derivatives of the field vary as $1/a^{n+1}$.

The above result suggests that for a fixed ratio of the distance from a coil to its radius, smaller coils are more effective at producing magnetic fields and gradients. However, if we let the ratio change and measure the distance uniformly, it becomes apparent that the field of smaller coils also dies out faster. Thus, there is a tradeoff between efficiency in generating a field and its absolute size, and for a given distance from the center of the coil there exists the optimal coil radii for producing the maximum field and its gradient at that point. We proceed to calculate these radii by setting the appropriate derivatives to zero. In all of the following cases the derivatives are taken with respect to the actual variables $a$ and $z$ even though the results are expressed in terms of the dimensionless factor $\xi$.

By setting $B_a \equiv 0$, we observe that for a given distance $z$ between a coil center and a point on its axis, the coil that has the radius

$$a^B \triangleq \operatorname{argmax}_a \{B(z,a)\} = \sqrt{2} \cdot z \simeq 1.4z \approx 3/2\, z \tag{3.20}$$

creates the largest field per unit current. Likewise, setting $B_{az} = B_{za} \equiv 0$, we obtain a similar result for the magnitude of the field gradient:

$$a^{\nabla} \triangleq \text{argmax}_a \left\{ \left| B_z(z,a) \right| \right\} = \sqrt{2/3} \cdot z \simeq 0.8z \approx 4/5\, z \,. \tag{3.21}$$

Finally, the optimal coil size for changing the field gradient is found from $\frac{\partial}{\partial a} B_{zz} \equiv 0$ :

$$8x^2 - 24x + 3 = 0 \rightarrow x^* = \frac{12 \pm \sqrt{12^2 - 4 \cdot 3 \cdot 8}}{2 \cdot 8} = 1.2, 0.3$$

$$a^{\partial\nabla} \triangleq \text{argmax}_a \left\{ \left| B_{zz}(z,a) \right| \right\} = \sqrt{x^*} \cdot z \simeq z, 1/2\, z \,. \tag{3.22}$$

## 3.4 Off-axis Magnetic Field[4]

The exact analytical expression for the off-axis magnetic field of a circular winding can be derived from the magnetic vector potential, expressed in spherical coordinates as

$$A_\phi(\rho,\theta) = \frac{\mu}{4\pi} I \oint \frac{dl}{r} = \frac{\mu}{4\pi} \frac{Ia}{\sqrt{\rho^2 + a^2}} \int_0^{2\pi} \frac{\cos\phi \, d\phi}{\sqrt{1 - \varepsilon \cos\phi}} \,, \tag{3.23}$$

where

$$\varepsilon = 2a\rho \sin\theta / \left( \rho^2 + a^2 \right),$$

and the rest of the elements are as defined in the figure below. For $\rho \gg a$ (near-field), $\rho \gg a$ (far-field), or $\sin\theta \ll 1$ (near the axis), $\varepsilon$ is small and the potential can be approximated as

[4] Adapted from [2], pp.110-121

$$A_\phi \cong \frac{\mu I a^2}{4} \frac{\rho \sin\theta}{\left(\rho^2 + a^2\right)^{3/2}} \quad . \tag{3.24}$$

The spherical components of the magnetic field $\mathbf{B} = \nabla \times \mathbf{A}$ are then simplified to

$$\begin{aligned} B_\rho(\rho,\theta) &= \frac{1}{\rho \sin\theta} \frac{\partial\left(\sin\theta A_\phi\right)}{\partial\theta} \cong \frac{\mu I a^2 \cos\theta}{2\left(\rho^2 + a^2\right)^{3/2}}, \\ B_\theta(\rho,\theta) &= -\frac{1}{\rho} \frac{\partial\left(\rho A_\phi\right)}{\partial\rho} \cong -\frac{\mu I a^2 \left(2a^2 - \rho^2\right)\sin\theta}{4\left(\rho^2 + a^2\right)^{5/2}}. \end{aligned} \tag{3.25}$$

Having obtained an approximate analytical expression for the field, we proceed to compute the exact field components, based on another analytical formula. From the symmetry of the problem, the toroidal and poloidal components of the magnetic vector potential are zero.[5] Converting the azimuthal component to cylindrical coordinates

$$z = \rho\sin\theta, \quad r = \rho\cos\theta$$

and introducing the parameter

$$k^2(z,r) = \frac{4ar}{(a+r)^2 + z^2}, \tag{3.26}$$

we obtain

$$A_\phi(z,r) = \frac{\mu I}{\pi k}\sqrt{\frac{a}{r}}\left[\left(1 - \frac{k^2}{2}\right)K - E\right], \tag{3.27}$$

where $K$ and $E$ are the complete elliptic integrals of the first and second kind, defined as

[5] From *Ampere's law*, $\nabla \times \mathbf{H} = \mathbf{j}$ and the potential is defined via $\mathbf{H} = \nabla \times \mathbf{A}$, where $\mathbf{j}$ is the current that generates the field $\mathbf{H}$ which is related to the flux density via $\mathbf{B} = \mu\mathbf{H}$. Because the current is contained in a plane, the potential is perpendicular to the plane and thus contains only azimuthal component.

$$K(k)=\int_0^{\pi/2}\left(1-k^2\sin^2 x\right)^{-1/2}dx,$$
$$E(k)=\int_0^{\pi/2}\left(1-k^2\sin^2 x\right)^{1/2}dx. \tag{3.28}$$

Magnetic field components are then obtained by differentiation:

$$B_z(z,r)=\frac{1}{r}\frac{\partial\left(rA_\phi\right)}{\partial r}=\frac{\mu I}{2\pi}\left[\left(a+r\right)^2+z^2\right]^{-1/2}\left[K+\frac{a^2-r^2-z^2}{\left(a-r\right)^2+z^2}E\right],$$
$$B_r(z,r)=-\frac{\partial A_\phi}{\partial z}=\frac{\mu I}{2\pi}\frac{z}{r}\left[\left(a+r\right)^2+z^2\right]^{-1/2}\left[-K+\frac{a^2+r^2+z^2}{\left(a-r\right)^2+z^2}E\right]. \tag{3.29}$$

These formulas apply both to 2-D and 3-D problems because **B** has only two components

$$\mathbf{A}_r=\mathbf{A}_z=0\ \rightarrow\ \mathbf{B}_\phi=0$$

and dependence on $\theta$ is removed by rotational symmetry: $\mathbf{B}(z,r,\theta)=\mathbf{B}(z,r)\ \forall\theta$. The values for the elliptic integrals are tabulated and easily obtainable on a computer. For that reason, equations 3.26 – 3.29 will form the basis for an exact numerical (MATLAB) simulation, which we will introduce in the next chapter.

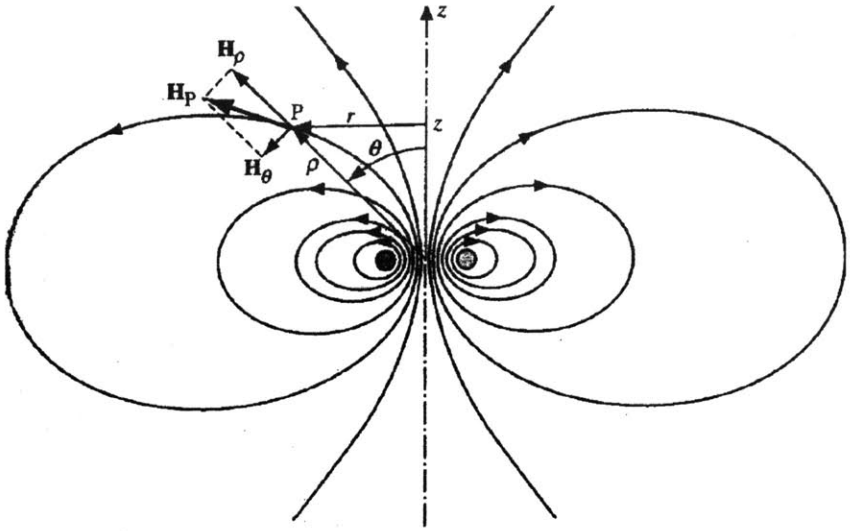


**Fig. 3.2 Magnetic Field of a Current Loop**[6]

## 3.5 The Field of a Thick Solenoid

This section is intended as a brief reference to the simulation software used for field computations. Our purpose here is to demonstrate how the fields were produced and to comment briefly on the results. The code that we chose for our computation is SOLDESIGN. It is a general purpose program for calculating and plotting magnetic fields and Lorentz forces for a system of coaxial, uniform current density solenoids. It was designed and tested at the Plasma Fusion Center at MIT. There are several versions available both for the VAX cluster system and for PC. We used the PC version, which is simplified via reduced dimensions and a lack of graphics, but is nevertheless perfectly adequate for our purposes.

[6] Reprinted from [1], p.93

Both the input and output to the program are passed in files of a certain format. The input consists of a sequence of commands that prescribe the geometry of a solenoidal coil and either the overall current density or the total ampere-turns of current flowing through it. When viewed in cross-section, the coil is represented by two rectangles of equal sizes and at equal distances from the origin. (*i.e.*, the center of the solenoid) The geometry is defined by specifying the coordinates of the lower left corner of the left rectangle, its thickness in the x- and y- directions (the radial and axial builds), and a symmetry parameter that allows to include certain reflections of the coils. (*e.g.*, a split pair) The output consists of the coordinates of the field points (the spatial grid), the flux, and the components of the magnetic flux density. A Gaussian quadrature algorithm is employed to integrate the flux and flux density components azimuthally around the perimeter of the coil. Additional details can be obtained from the SOLDESIGN User's Manual available at the Plasma Fusion Center at MIT.

In our setup, the coil is a solenoid of radius 60cm (the average of the inner and outer radii) with square cross-section of 8 cm on the sides and a total current of 500kA-turns flowing through it. The field is computed on a rectangular grid of 61x61 points with the corners at (-31,6), (29,6), (-31,79), and (29,79) cm measured away from the center of the coil. The overall arrangement contains four such coils positioned along the sides of an 80cm square. Because our goal is to analyze the performance of a multi-coil system, we are considering only those regions of space where more than one coil can make a significant contribution to the total magnetic field, given the maximum allowable current levels. Therefore, the operating region does not include 6cm strips adjacent to each of

the coils, because inside these strips, the closest coil dominates all others and the problem of controlling the fields effectively reduces to one dimension. For the multidimensional problem that we are considering, the fields of all the coils are superposed and scaled by their respective current levels. In a later section, we will define how the field values computed for one coil are weighted, rotated, and superposed to produce the fields in a multi-coil arrangement.

## 3.6 Analytical Approximation

The finite element code presented above produces the most accurate result of all the other methods considered. However, it's disadvantage is that the field values are computed on a discrete spatial grid and a continuous interpolation scheme is required to calculate the fields at all other points in the operating region. There are many general numerical techniques available for that purpose, but it behooves us to attempt a specialized approach by approximating the field on the entire spatial grid by a single analytical function with relatively few parameters. Some precision is necessarily compromised in the process, but the benefits outweigh the losses. First, the computation time is shortened dramatically due to the significant reduction in the complexity of the problem. Second, the resultant expression is simple enough to facilitate analytical approaches to the dynamical analysis and control strategies. In particular, the state-space system of equations can then be expressed and analyzed in a functional form.

There is no reason to expect that dynamical behavior of the system will actually conform to a certain known elementary function; in the most general case, we will merely have a

table of values. A standard approach in such situation would be to approximate the table with a series or an integral of some simple and well-behaved basis functions. However, there is no guarantee on the rate of convergence of these sums, even if the data is reasonably orderly. Furthermore, such representation will not likely be sufficiently intuitive to contribute to the qualitative description of the system. The approach that we have chosen is designed to reflect the qualitative features of our system. For that reason, it is less systematic and, potentially, less precise than a quantitative method. However, we will demonstrate with our approach that considerable numerical accuracy can be achieved without significant increase in the complexity of the model.

### 3.6.1 The Radial Field Component

The output of the SOLDESIGN is shown in the figure below. The mesh is made crude for enhanced visibility of the individual waveforms. The field is shown in Tesla.

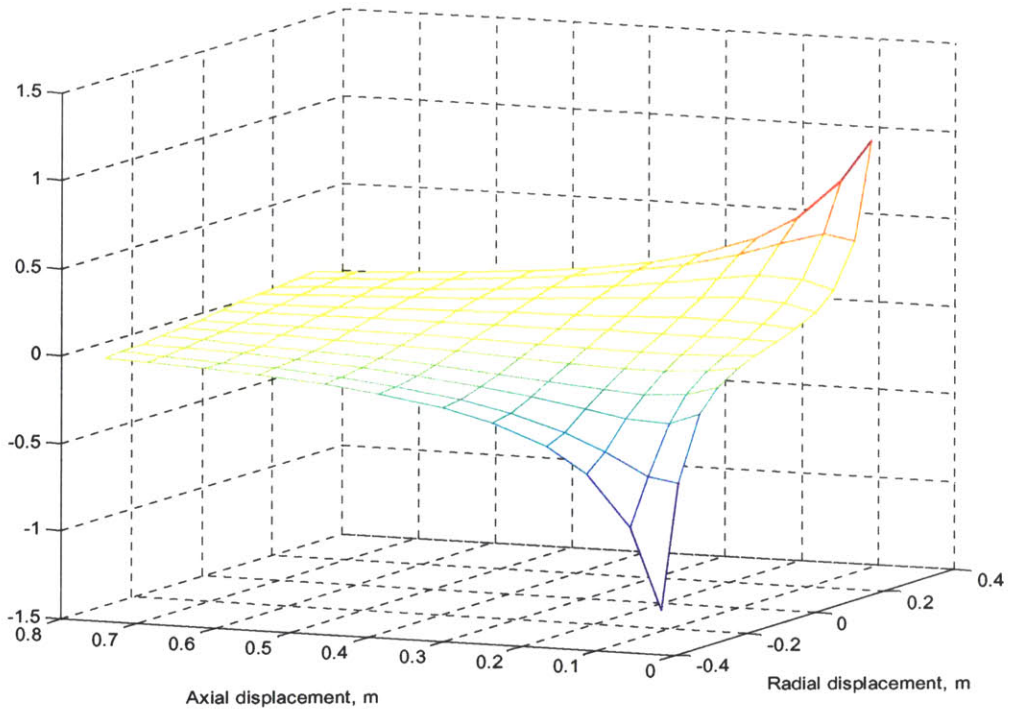


**Fig. 3.3 Radial Field Component**

The shape of the mesh lines suggests that the field is exponentially decaying in the axial (y-) direction and follows an odd-power polynomial in the radial (x-) direction. Focusing on the particular mesh lines, we observe that the exponential curve also has a peak and appears to consist both of the decay function and of its derivative. This type of behavior is characteristic of the critically damped systems, that have time evolution $f(t) = p_{oly}(t) \cdot e^{-t/\tau}$. For simplicity, we will limit our consideration to the first- and second-order polynomials.

$$B_x(x,y) = p_0(x)e^{-y/\kappa_0} + p_1(x)ye^{-y/\kappa_1} + p_2(x)y^2e^{-y/\kappa_2}. \tag{3.30}$$

Alternatively, we can first look at the polynomials in $x$. A typical profile is presented in the figure 1.3. The function appears anti-symmetric around the $B$-axis and its slope near the origin is sufficiently non-flat to suggest a low degree polynomial, like 3rd or $5^{th}$ order.

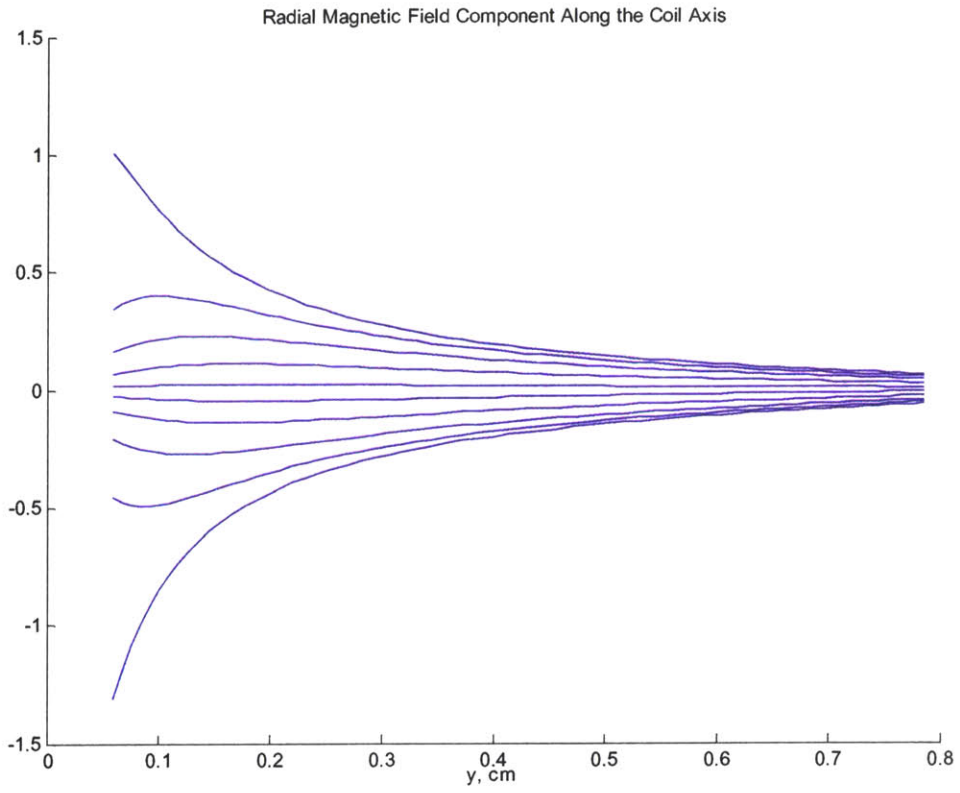


**Fig. 3.4 Radial Field Profiles**

Because polynomials are easier to approximate than the product of polynomials and exponentials, we have chosen to model the field as

$$B_x(x,y) = c_0(y)x^5 + c_1(y)x^3 + c_2(y)x \tag{3.31}$$

Therefore, for each value of $y = y^*$ we approximate $B_x(x,y^*)$ by a polynomial of the $5^{th}$ degree in the odd powers of x. The algorithm to retrieve coefficients $\{c_0, c_1, c_2\}$ is MATLAB's non-linear best fit, *nlinfit*, based on Newton's method. It is convenient to

use when the functional form of the approximation is well known and is neither a pure polynomial nor an invertible function of one. (such as $e^{p(x)}$)

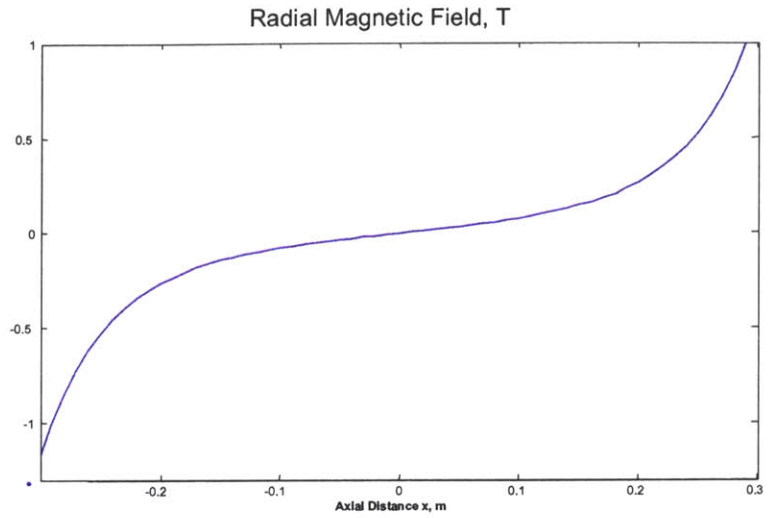


**Fig. 3.5 Radial Magnetic Field (Radial Slice)**

The function *nlinfit* requires four inputs: the values of the independent and dependent variables; the functional expression relating the two, with unknown but adjustable coefficients; and the initial values of the coefficients. The nature of the method is such that its performance depends substantially on the quality of the initial guess of these coefficients. Therefore, we have adopted an iterative/recursive scheme where the coefficients are first iterated through a crude list of plausible values and the most accurate representation is chosen. Then, starting with the corresponding initial values, the program is run recursively, where the answer from the previous iteration is taken as the input to the next one. The entire procedure is then repeated for each value of $y$, so that the coefficients are themselves functions of $y$, as shown in Eqn. 3.31 and in Fig. 3.6,7.

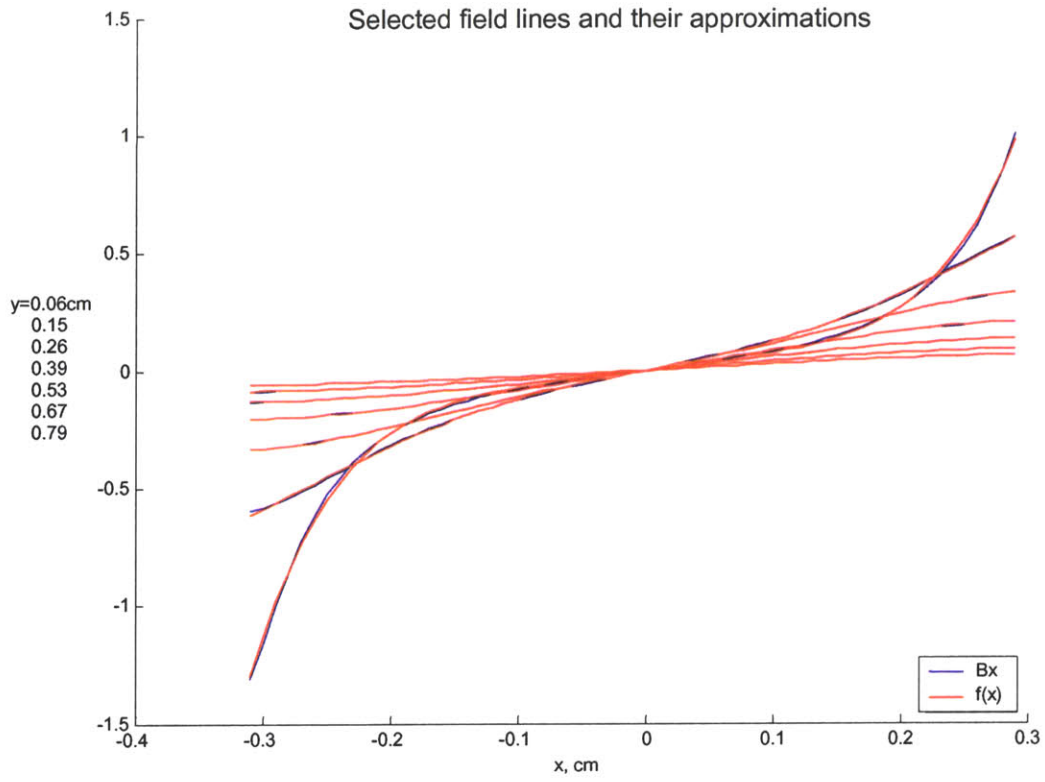


**Fig. 3.6 Radial Field Approximations**

As expected from the above analysis, the coefficient curves resemble impulse response of a critically damped system – that is they appear like a product of exponential and polynomial functions of variable $y$. The fitting is done the same way as for $x$, with the exception that a different functional relationship is chosen to estimate the coefficients. $c_0$ and $c_2$ are estimated with $f(y) = a_0 e^{-k_0 y} + a_1 y e^{-k_1 y}$, while $c_1$ is estimated with $g(y) = b_0 e^{-m_0 y} + b_1 y e^{-m_1 y} + b_2 y^2 e^{-m_2 y}$. In total, $B_x(x,y)$ is represented with 14 numbers and has the form:

$$B_x(x,y) = [a_{00}e^{-k_{00}y} + a_{01}ye^{-k_{01}y}]x^5 + [a_{10}e^{-k_{10}y} + a_{11}ye^{-k_{11}y} + a_{12}y^2e^{-k_{12}y}]x^3 + [a_{20}e^{-k_{20}y} + a_{21}ye^{-k_{21}y}]x$$

where the coefficients are:

| $a_{00}$ | $a_{01}$ | $a_{10}$ | $a_{11}$ | $a_{12}$ | $a_{20}$ | $a_{21}$ | $k_{00}$ | $k_{01}$ | $k_{10}$ | $k_{11}$ | $k_{12}$ | $k_{20}$ | $k_{21}$ |
|---|---|---|---|---|---|---|---|---|---|---|---|---|---|
| -1.53e4 | 2e3 | -433 | 1451 | -99.4 | 12.42 | 0.26 | 14 | 15 | 7.7 | 13.5 | 14.9 | 5.04 | 1.23 |

**Table 1: Radial Field Coefficients**

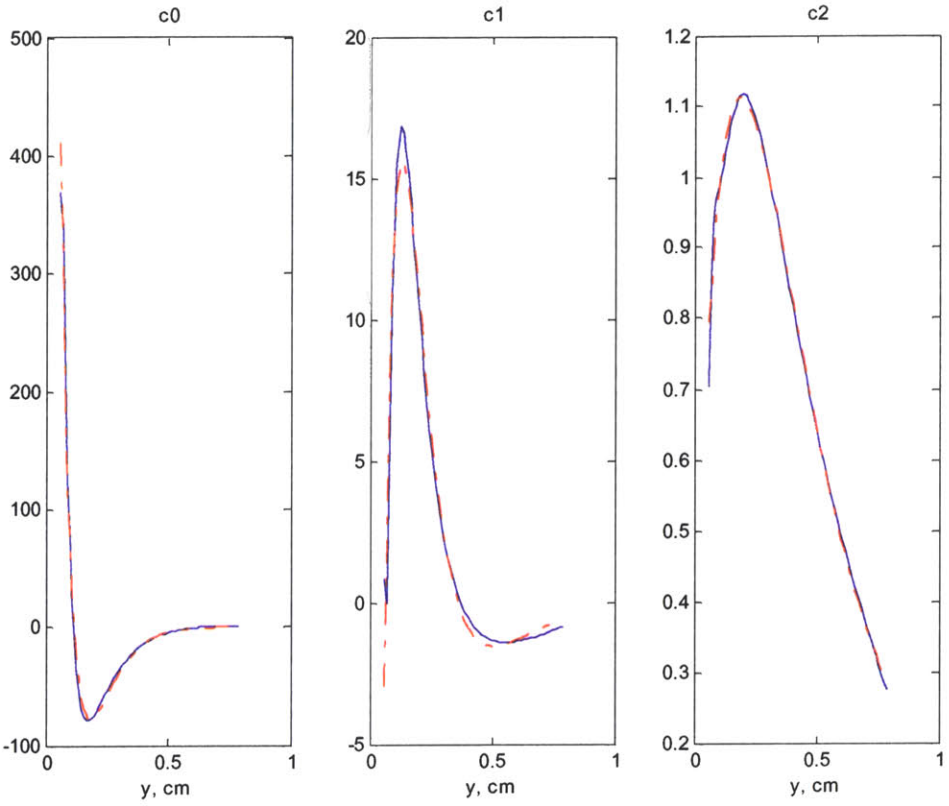


**Fig. 3.7 Radial Field Coefficients**

The resulting error in the radial field is computed as $e_x = B_x(x,y) - \tilde{B}_x(x,y)$, where the second term represents the SOLDESIGN field and the first represents its approximation.

It is apparent that the error can be bounded to within 10% of its maximum value for most of the operating region and for $y > 20\text{cm}$ it can be further contained by a factor of two. This result is very promising, considering that we are replacing $61^2 = 3721$ numbers with mere 14. With the knowledge of error bounds, we can design robust controllers that are capable of operating with imprecise but bounded measurements of the field. In reality, if the error in the real measurements does not exceed these 10%, the controllers would accommodate both the error in modeling and the errors in the sensor readings.

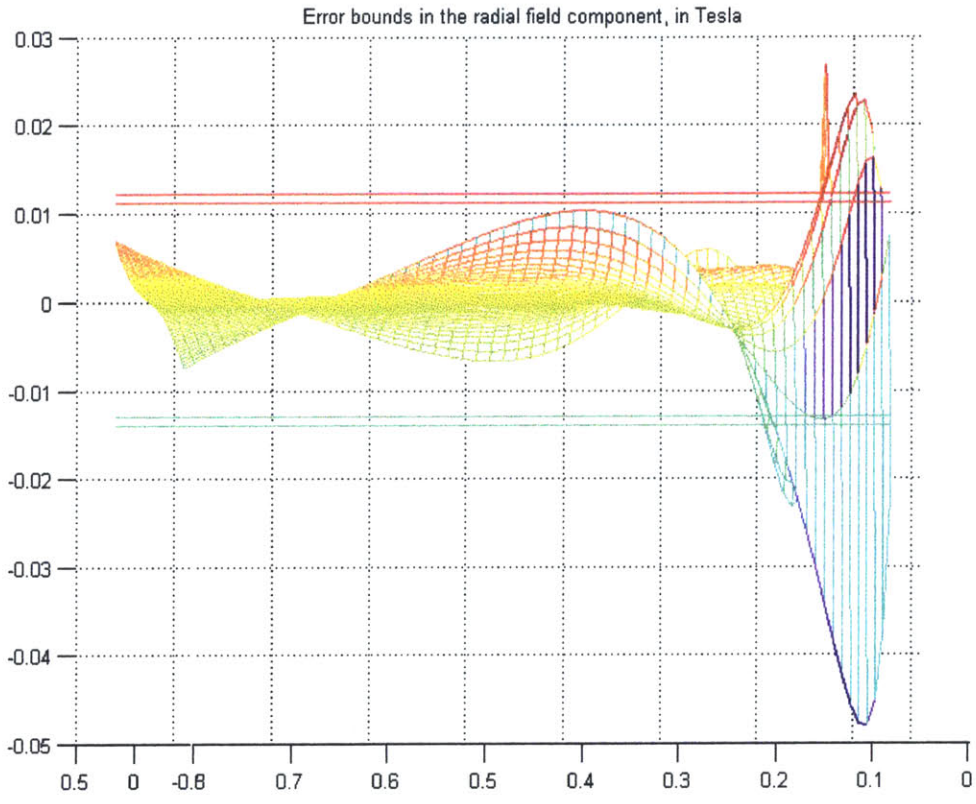


**Fig. 3.8 Radial Field Approximation Error**

### 3.6.2 The Axial Field Component

The approach is the same as for the radial component. First, the shape of the field is determined both in the radial and in the axial cross-sections. Then, the simpler of the two representations is considered and its coefficients are computed as a function of the other variable. Then, similar fitting is performed for each of the coefficients.

The axial field is represented as a mesh in Fig. 3.9.

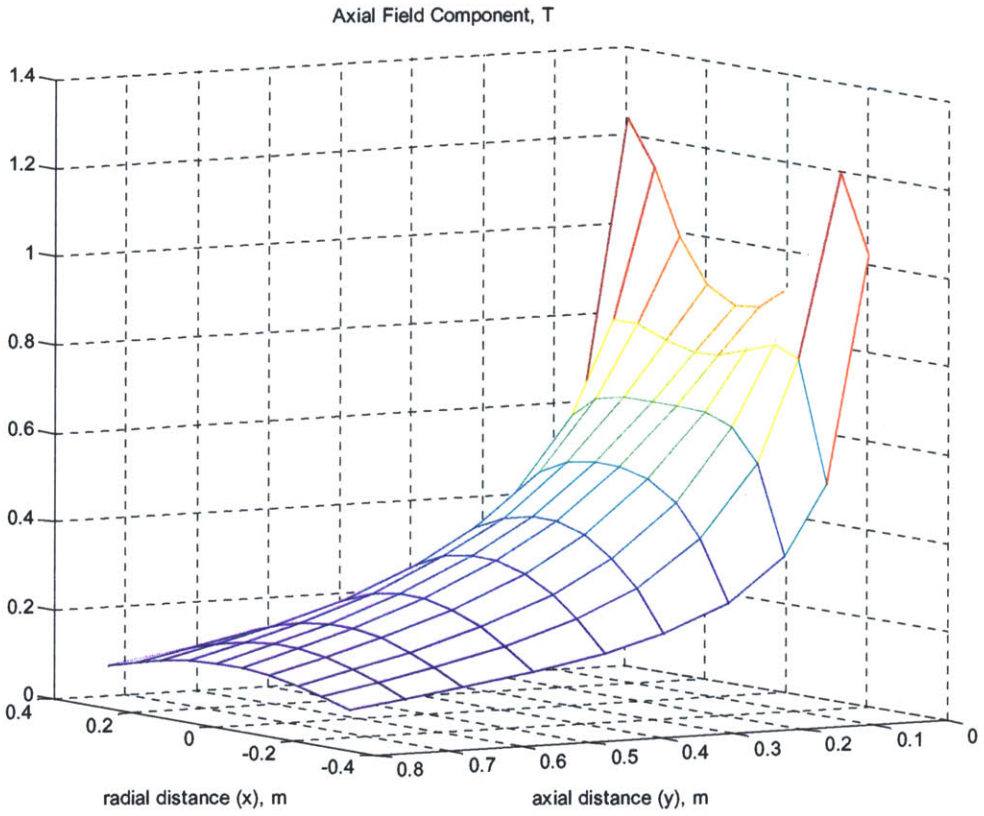


**Fig. 3.9 Axial Field Component**

Just like the radial field component, the axial one falls off exponentially in the axial direction. However, unlike the radial component, it follows an even-powered polynomial

in the radial direction. Approximating the field in the axial direction with the sum of products of exponential and polynomial functions, we obtain

$$B_y(x,y) = a_0(x)ye^{-k_0(x)\cdot y} + a_1(x)e^{-k_1(x)\cdot y} \tag{3.32}$$

The coefficients are then fitted with a polynomial in the even powers of $x$. As shown in Fig. 3.10, the results are not very promising because the coefficients vary sporadically and cannot be easily approximated with polynomials. Some of them ( $a_0$ and $a_1$ ) actually vary exponentially in the steep regions and polynomially in the valley around the origin.

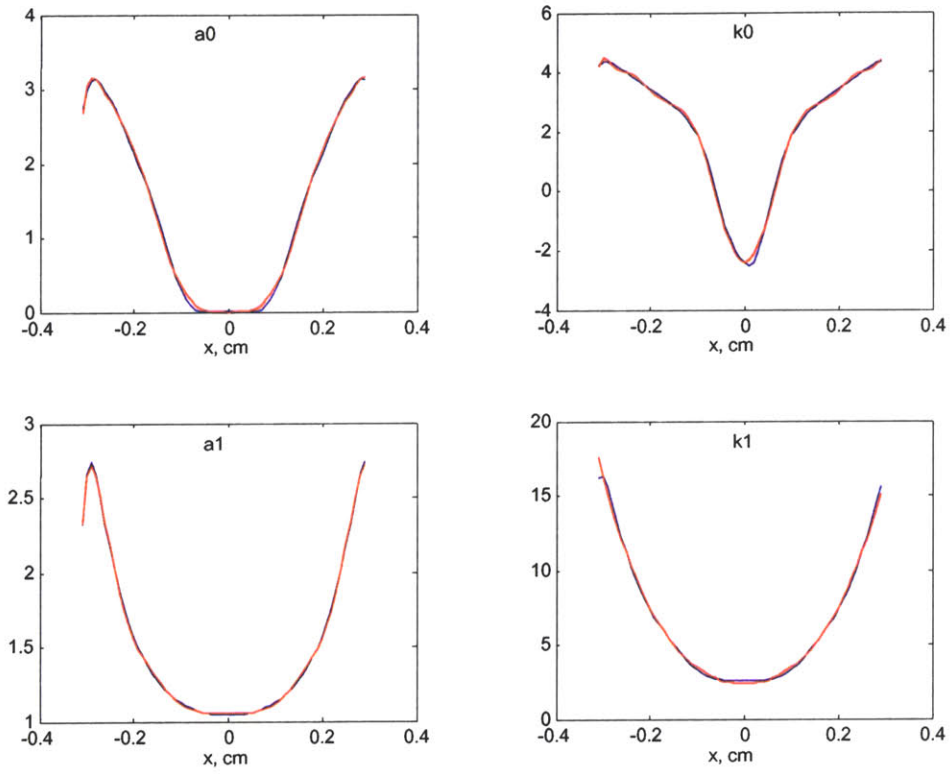


**Fig. 3.10 Axial Field Coefficients (axial)**

Alternatively, we can first approximate the axial field in the radial direction and then fit the coefficients along the $y$-axis. As evidenced in Fig. 3.11, the functions of $x$ are all

even and $B_y$ can be approximated directly as a polynomial in $x^2$. Furthermore, we can try to normalize either $x$ or $x^2$ by their variances to obtain a better fit with fewer coefficients.

The procedure for polynomial approximation is more straightforward than *nlinfit*. First, the Vandermonde matrix $V$ is formed, whose elements are the powers of $\xi = x^2$.

$$V_{i,j} = \xi_i^{n-j}, \tag{3.33}$$

where $n$ is the largest power of $\xi$ and thus $2n$ is the largest power of $x$. Then, the coefficient vector, **p**, is a solution to the least-squares problem:

$$\mathbf{p} = \mathbf{V}^{-1} \cdot \mathbf{y} = (\mathbf{Q} \cdot \mathbf{R})^{-1} \cdot \mathbf{y} = \mathbf{R}^{-1} \cdot \mathbf{Q}^{-1} \cdot \mathbf{y} = \mathbf{R}^{-1} \cdot \mathbf{Q}^{\mathrm{T}} \cdot \mathbf{y}, \tag{3.34}$$

where **y** is the vector of data points and QR-factorization (Cholesky) decomposes **V** into an orthonormal matrix **Q** and an upper-triangular matrix **R**. It is, essentially, an instance of the Gram-Schmidt orthogonalization, where

$$\mathbf{V} = \begin{bmatrix} & & \\ v_1 & v_2 & v_3 \cdots \\ & & \end{bmatrix} = \begin{bmatrix} & & \\ q_1 & q_2 & q_3 \cdots \\ & & \end{bmatrix} \begin{bmatrix} q_1^{\mathrm{T}} v_1 & q_1^{\mathrm{T}} v_2 & q_1^{\mathrm{T}} v_3 & \vdots \\ & q_2^{\mathrm{T}} v_2 & q_2^{\mathrm{T}} v_3 & \vdots \\ & & q_3^{\mathrm{T}} v_3 & \vdots \\ & & & \ddots \end{bmatrix} = \mathbf{QR}, \tag{3.35}$$

and the columns of **Q** are chosen so that $q_1$ is in the direction of $v_1$, $q_2$ is in the plane of $v_1$ and $v_2$, etc. The key is to make **R** invertible, which will happen whenever the number of data points is greater than the degree of the polynomial and whenever the data points are not repeated. Normalizing the data can also effect the conditioning of **R** and so, we will consider the polynomials in

$$\xi = x^2, \quad \gamma = x^2 \Big/ \sigma_{x^2} = \frac{x^2}{\text{std}(x^2)}, \quad \text{and} \quad \lambda = x^2 \Big/ \sigma_x{}^2 = \frac{x^2}{\text{var}(x)}.$$

The data is not centered because the coefficient functions are already symmetrical around the origin. The least-square procedure thus projects, one by one, the powers of $x$ onto the data, so that at each step, the approximation error is orthogonal to all the powers considered.

The first five terms in the polynomial expansion were sufficient to approximate the field to within several percents of its nominal value. The coefficient functions are displayed for three different representations of data in Fig. 3.12. Certain complications arise when the data is not normalized. For example, there is a large spread in the coefficient values even though, as verified experimentally, all five coefficients are needed to achieve a reasonable fit. The first representation is thus discounted and the other two are compared. As expected, they appear fairly similar in coefficient values, although the waveforms in the third representation are slightly more amiable to approximation. Therefore, the third approximation is chosen and curve fitting is performed with *nlinfit* using exponential-polynomial functions of the type considered above. (Eqn. 3.32)

The axial component of the field is then approximated as

$$
\begin{aligned}
B_y(x,y) = &\left\{a_{00}e^{-k_{00}y} + a_{01}ye^{-k_{01}y}\right\}\left(\frac{x}{\sigma_x}\right)^8 \\
&+\left\{a_{10}e^{-k_{10}y} + a_{11}ye^{-k_{11}y}\right\}\left(\frac{x}{\sigma_x}\right)^6 \\
&+\left\{a_{20}e^{-k_{20}y} + a_{21}ye^{-k_{21}y}\right\}\left(\frac{x}{\sigma_x}\right)^4 \\
&+\left\{a_{30}e^{-k_{30}y} + a_{31}ye^{-k_{31}y}\right\}\left(\frac{x}{\sigma_x}\right)^2 \\
&+\left\{a_4e^{-k_4y}\right\},
\end{aligned}
\tag{3.36}
$$

where

$$
\sigma_x \triangleq \text{std}(x) = \frac{1}{x_{\max} - x_{\min}}\sum(x-\bar{x})^2,
$$

$$
\bar{x} \triangleq \text{avg}(x) = \frac{x_{\max} - x_{\min}}{2}.
$$

There axial field is thus represented with 18 coefficients. Their values are:

| $a_{00}$ | $a_{01}$ | $a_{10}$ | $a_{11}$ | $a_{20}$ | $a_{21}$ | $a_{30}$ | $a_{31}$ | $a_4$ |
|---|---|---|---|---|---|---|---|---|
| 5.33 | -0.36 | -39.27 | 2.04 | 72.29 | -2.92 | -2.11 | 0.37 | 1.04 |
| $k_{00}$ | $k_{01}$ | $k_{10}$ | $k_{11}$ | $k_{20}$ | $k_{21}$ | $k_{30}$ | $k_{31}$ | $k_4$ |
| 23.81 | 19.35 | 24.19 | 18.12 | 23.89 | 15.16 | 5.40 | 5.36 | 2.54 |

**Table 2: Axial Field Coefficients**

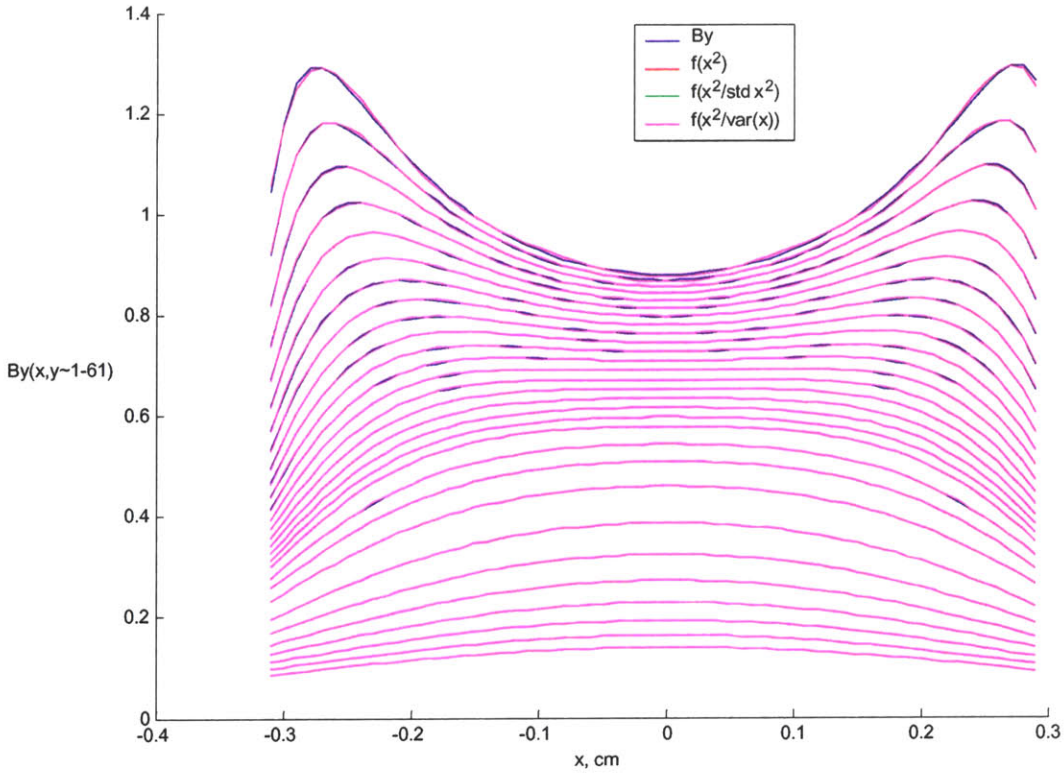


**Fig. 3.11 Axial Field Profiles**

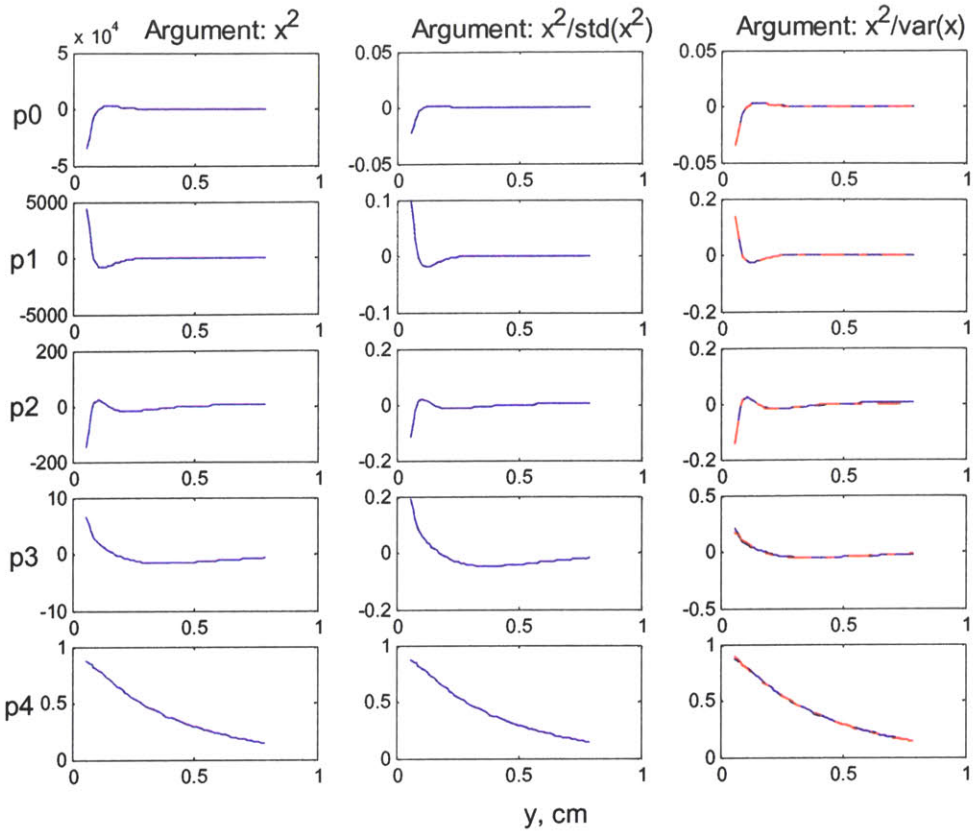


**Fig. 3.12 Axial Field Coefficients (radial)**

The error in the axial field approximation is $e_y = B_y(x,y) - \tilde{B}_y(x,y)$, where the first term represents the approximation and the second – the nominal field obtained with SOLDESIGN. It is bounded between –0.017 and 0.004 Tesla, which is again within 10% of the field's maximum value for the part of the operating region with $y > 20$cm. Furthermore, it can be contained by another factor of two for $y > 30$cm. In this case, the $61 \times 61$ grid is replaced by a total of 18 numbers, as opposed to 14 for the radial field component. However, the error bounds thus obtained are also a bit tighter: 0.021 vs. 0.025. Once again, it is reasonable to expect that the other uncertainties

in the system will have at least a 10% error bound and so, the approximation error will not be a major hurdle in the design of a robust controller.

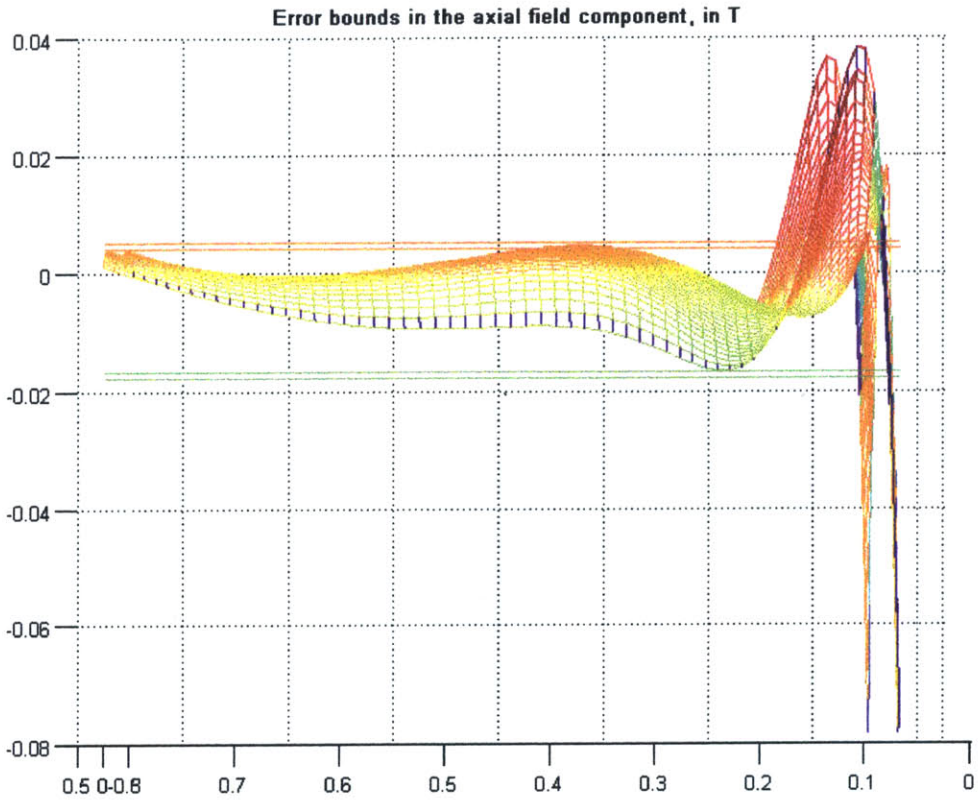


**Fig. 1.13 Axial Field Approximation Error**

# Chapter 4

# Control of Magnetic Manipulators

## 4.1 Single Input Dynamics

In Chapter 2, we have formulated the equations of motion of a magnetic dipole in the presence magnetic field. For convenience, we repeat them here:

$$\begin{aligned} \mathbf{F} &= \nabla(\mathbf{p}\cdot\mathbf{B}) \\ \mathbf{T} &= \mathbf{p}\times\mathbf{B} \end{aligned} \tag{4.1}$$

The dipole experiences a torque that tends to align its magnetic moment with the direction of the field and a force that tend to accelerate it in the direction of the field gradient. Assuming that rotational motion will entirely precede translation for any appreciable angle between the dipole and the field, (this assumption has been quantify in the previous chapters and also verified experimentally for a variety of dynamic scenarios) we can approximate the dipole moment of the magnet in the force equation via

$$\mathbf{p} \simeq p\cdot\hat{\mathbf{B}} = \frac{p}{B}\mathbf{B} \tag{4.2}$$

Therefore, magnetic force acting on the dipole can be expressed as

$$\mathbf{F} \simeq \nabla\left(\frac{p}{B}\mathbf{B}\cdot\mathbf{B}\right) = p\nabla\left(\frac{B^{\not 2}}{\not B}\right) = p\cdot\nabla B, \quad \text{where } B \triangleq \|\mathbf{B}\|. \tag{4.3}$$

The field acting on a dipole is a function of the spatial coordinates of its center of mass. It is also dependent on the location, orientation, and the strength of the field sources. In our formulation, the sources are always fixed in place, so that their only controllable attribute is their strength, which can be manipulated by adjusting the currents in the coils. In the last chapter, we have shown that for a single solenoid, the strength of the field is proportional to the total current flowing through the coil cross-section. Therefore, in the most general terms, the field can be expressed as

$$\mathbf{B}(\mathbf{s}) = \vec{h}(\mathbf{s})\cdot i, \tag{4.4}$$

where $\mathbf{s}$ contains the coordinates of the dipole's center of mass, $i$ is the coil current, and $\vec{h}(\mathbf{s})$ is the field for at the location of the dipole for a unit current in the coil.

If the dipole's state consists of its location, orientation, and the linear and angular velocities, then the state evolution can be described by the following dynamical system:

$$\begin{cases} \dot{\mathbf{s}} = \mathbf{v}, \quad \dot{\varphi} = \omega \\ \dot{\mathbf{v}} = \mathbf{F}\Big/ m \simeq \dfrac{p}{m}\cdot\nabla\|\mathbf{B}\| = \dfrac{M}{\rho}\cdot\nabla\left\|\vec{h}(\mathbf{s})\right\| i \\ \dot{\omega} = \mathbf{T}/I = \dfrac{\mathbf{p}\times\mathbf{B}}{I} = \dfrac{p}{I}\left[\hat{\mathbf{p}}(\varphi)\times\vec{h}(\mathbf{s})\right] i \end{cases} \tag{4.5}$$

## 4.2 Superposition of Inputs

The system presented above is severely over-determined because it contains only one input, which means that the space of the achievable state trajectories is one dimensional. In this section, we consider the superposition of several inputs to improve the controllability of the system. For simplicity of exposition, the problem will be formulated in two-dimensional Eucledian space; however, all derivations are presented in a general, vector form, and so extension to three dimensions should be relatively straightforward. The following notational convention shall be adopted. The dipole is located at a point **s** in space; a particular coil of radius $a$ is centered at **c** with the normal vector oriented at an angle $\theta$ with the $y$-axis; a unit-radius circular winding centered at the origin, with the normal pointing along the positive $y$-axis and with current $i$ flowing through it, produces the field at **s** is described by the Eqn. 4.4.

In the frame of reference of the coil at $\{\mathbf{c},\theta\}$, the point **s** appears to be at

$$\mathbf{s}^* = \mathcal{R}_{-\theta}\{(\mathbf{s}-\mathbf{c})\}, \quad \mathcal{R}_\theta \triangleq \mathrm{rot}_\theta = \begin{pmatrix} \cos\theta & -\sin\theta \\ \sin\theta & \cos\theta \end{pmatrix}, \quad \mathcal{R}_{-\theta} = \mathcal{R}_\theta^{\mathrm{T}}. \tag{4.6}$$

The field generated by the coil at $\mathbf{s}^*$, expressed in the coil's frame of reference, is

$$\mathbf{B}^*(\mathbf{s}^*) = \vec{h}(\mathbf{s}^*)\,i = \vec{h}(\mathcal{R}_{-\theta}\cdot\mathbf{s} - \mathcal{R}_{-\theta}\cdot\mathbf{c})\,i = \vec{h}(\mathcal{R}_{-\theta}\cdot\mathbf{s} - \mathbf{r})\,i, \quad \text{where } \mathbf{r} \triangleq \mathcal{R}_{-\theta}\cdot\mathbf{c}. \tag{4.7}$$

In the standard frame of reference,

$$\mathbf{B}(\mathbf{s}) = \mathcal{R}_\theta \cdot \mathbf{B}^*(\mathbf{s}^*) = \mathcal{R}_\theta \cdot \vec{h}(\mathcal{R}_{-\theta}\cdot\mathbf{s} - \mathbf{r})\,i$$

$$\boxed{\mathbf{B}(\mathbf{s}) = \mathcal{R}_\theta \cdot \vec{h}\{\mathcal{R}_{-\theta}\cdot(\mathbf{s}-\mathbf{c})\}\,i} \tag{4.8}$$

If $\vec{h}(\cdot)$ is approximated by a linear function,

$$\vec{h}(\mathbf{s}) \simeq \mathbf{J} \cdot (\mathbf{s} - \mathbf{s}_0) = \mathbf{J} \cdot \mathbf{s} + K, \tag{4.9}$$

where

$$\mathbf{J} \triangleq \frac{d\vec{h}}{d\mathbf{s}} = \begin{pmatrix} f_x & f_y \\ g_x & g_y \end{pmatrix} \tag{4.10}$$

is the Jacobian matrix for the system, then the linearized field is

$$\begin{aligned} \tilde{\mathbf{B}}(\mathbf{s}) &= \left\{ \mathcal{R}_\theta \cdot A \cdot \mathcal{R}_{-\theta} \cdot \mathbf{s} - \mathcal{R}_\theta \cdot A \cdot \mathbf{r} + \mathcal{R}_\theta \cdot K \right\} i \\ &= \left\{ \mathbf{A}^\theta \cdot (\mathbf{s} - \mathbf{c}) + \mathbf{K}^\theta \right\} i, \end{aligned} \tag{4.11}$$

where $\mathbf{A}^\theta \triangleq \mathcal{R}_\theta \cdot A \cdot \mathcal{R}_{-\theta}$, $\mathbf{K}^\theta \triangleq \mathcal{R}_\theta \cdot K$.

Because differentiation is a linear operation, it commutes with multiplication by a constant matrix or a vector. This circumstance considerably simplifies the derivation of a general expression for the field gradient of a coil. In fact,

$$\begin{aligned} \mathbf{s}^* &= \mathcal{R}_{-\theta} \cdot (\mathbf{s} - \mathbf{c}) \quad \text{and} \quad \mathbf{B} = \mathcal{R}_\theta \cdot \mathbf{B}^*, \\ \delta\mathbf{s}^* &\simeq \mathcal{R}_{-\theta} \cdot \delta\mathbf{s} \quad \text{and} \quad \delta\mathbf{B} \simeq \mathcal{R}_\theta \cdot \delta\mathbf{B}^*. \end{aligned} \tag{4.12}$$

Furthermore,

$$\delta\mathbf{B}^* \simeq \mathbf{J} \cdot \delta\mathbf{s}^* \cdot i. \tag{4.13}$$

Thus,

$$\delta\mathbf{B} = \mathcal{R}_\theta \cdot \delta\mathbf{B}^* \simeq \mathcal{R}_\theta \cdot \mathbf{J} \cdot \delta\mathbf{s}^* \cdot i = \underbrace{\mathcal{R}_\theta \cdot \mathbf{J} \cdot \mathcal{R}_{-\theta}}_{\mathbf{J}^\theta} \cdot \delta\mathbf{s} \cdot i. \tag{4.14}$$

Finally,

$$\nabla\mathbf{B} = \frac{\partial \mathbf{B}}{\partial \mathbf{s}} = \lim_{\delta\mathbf{s}\to 0}\left(\delta\mathbf{B} \setminus \delta\mathbf{s}\right) = \lim_{\delta\mathbf{s}\to 0}\left\{\left(i\cdot\mathbf{J}^{\theta}\cdot\delta\mathbf{s}\right)\cdot\delta\mathbf{s}^{-1}\right\} = \mathbf{J}^{\theta}\cdot i$$

$$\boxed{\nabla\mathbf{B} = \mathbf{J}^{\theta} i = \left[\mathcal{R}_{\theta}\frac{\partial \vec{h}}{\partial \mathbf{p}}\mathcal{R}_{-\theta}\right] i} \tag{4.15}$$

It remains to determine the scaling of the field with the radius. The following derivation is based on the field equations for a unit winding and, therefore, is only approximately valid for a finite-size coil. However, unless field measurements are taken at points very close to the coil, (which are not considered in the operating region of interest) the validity of such approximation is maintained, as has been verified experimentally. With the scaling coordinate transformation:

$$\rho = r/a, \quad \zeta = z/a, \tag{4.16}$$

the field equations (1.54) take the form

$$B_z(\zeta,\rho) = \frac{1}{r}\frac{\partial\left(rA_{\phi}\right)}{\partial r} = \frac{\mu I}{2\pi}a^{-1}\left[\left(1+\rho\right)^2+\zeta^2\right]^{-1/2}\left[K+\frac{1-\rho^2-\zeta^2}{\left(1-\rho\right)^2+\zeta^2}E\right]$$

$$B_r(\zeta,\rho) = -\frac{\partial A_{\phi}}{\partial z} = \frac{\mu I}{2\pi}a^{-1}\frac{\zeta}{\rho}\left[\left(1+\rho\right)^2+\zeta^2\right]^{-1/2}\left[-K+\frac{1+\rho^2+\zeta^2}{\left(1-\rho\right)^2+\zeta^2}E\right]$$

so that

$$\mathbf{B}^{a}(z,r) = a^{-1}\cdot\mathbf{B}\left(z/a, r/a\right). \tag{4.17}$$

Likewise, the gradient of the field scales inversely with the square of coil radius. Therefore,

$$\nabla\mathbf{B}^{a}(z,r) = a^{-2}\cdot\nabla\mathbf{B}\left(z/a, r/a\right). \tag{4.18}$$

Hence, for a circular coil of radius $a$, centered at $\mathbf{c}$, with the normal vector oriented at an angle $\theta$ with the $y$-axis, and with the total current $i$ flowing through it, the magnetic field and its gradient at a point $\mathbf{s}$ can be expressed as

$$\boxed{\begin{aligned}\mathbf{B}^a(\mathbf{s}) &= a^{-1}\mathcal{R}_\theta \cdot \vec{h}\{\mathcal{R}_{-\theta}\cdot(\mathbf{s}-\mathbf{c})/a\}\, i \\ \nabla\mathbf{B}^a(\mathbf{s}) &= a^{-2}\mathcal{R}_\theta \frac{\partial \vec{h}}{\partial \mathbf{s}}\left\{\mathcal{R}_{-\theta}\cdot(\mathbf{s}-\mathbf{c})/a\right\}\mathcal{R}_{-\theta}\, i\end{aligned}} \tag{4.19}$$

The functional form of $\vec{h}(\cdot)$ depends on the method of field calculation and on the type of the coil used. The equation is also valid for non-circular coils and, in general, for any field source (electromagnetic or permanent), so long as the coil parameters: $a$, $\mathbf{c}$, $\theta$, and $i$ are defined appropriately.

Extending the above results to a multi-coil (multi-source) system with general parameters

$$\mathscr{P} \triangleq \{a_n, c_n, \theta_n, i_n\}_{n=1\ldots N},$$

we obtain general 3rd order tensor expressions for the total field and its gradient at some point $\mathbf{s}$ in the operating region. Each 2nd order component in these expressions represents a matrix equation for the individual components of the field and gradient vectors.

$$\mathbf{B}_{tot}(\mathbf{s}) = \sum_{n=1}^{N} \mathbf{B}_n(\mathbf{s}) = \underbrace{\begin{bmatrix} a_1^{-1}\mathcal{R}_{\theta_1} \cdot \vec{h}\,\{\mathcal{R}_{-\theta_1} \cdot (\mathbf{s}-\mathbf{c}_1)/a_1\} \\ \vdots \\ a_N^{-1}\mathcal{R}_{\theta_N} \cdot \vec{h}\{\mathcal{R}_{-\theta_N} \cdot (\mathbf{s}-\mathbf{c}_N)/a_N\} \end{bmatrix}}_{\tilde{\mathbf{G}}} \cdot \underbrace{\begin{bmatrix} i_1 \\ \vdots \\ i_N \end{bmatrix}}_{\mathbf{i}} = \tilde{\mathbf{G}} \cdot \mathbf{i}$$

$$\nabla \mathbf{B}_{tot}(\mathbf{s}) = \sum_{n=1}^{N} \frac{\partial \mathbf{B}_n}{\partial \mathbf{s}}(\mathbf{s}) = \underbrace{\begin{bmatrix} a_1^{-2}\mathcal{R}_{\theta_1} \dfrac{\partial \vec{h}}{\partial \mathbf{s}}\left\{\mathcal{R}_{-\theta_1} \cdot (\mathbf{s}-\mathbf{c}_1)/a_1\right\}\mathcal{R}_{-\theta_1} \\ \vdots \\ a_N^{-2}\mathcal{R}_{\theta_N} \dfrac{\partial \vec{h}}{\partial \mathbf{s}}\left\{\mathcal{R}_{-\theta_N} \cdot (\mathbf{s}-\mathbf{c}_N)/a_N\right\}\mathcal{R}_{-\theta_N} \end{bmatrix}}_{\tilde{\mathbf{D}}} \cdot \underbrace{\begin{bmatrix} i_1 \\ \vdots \\ i_N \end{bmatrix}}_{\mathbf{i}} = \tilde{\mathbf{D}} \cdot \mathbf{i} \tag{4.20}$$

## 4.3 MIMO Controller

Equations 4.8 and 4.20 together describe the dynamics of the multiple-input multiple-output (MIMO) dynamical system. The equations are linear in the inputs and nonlinear in the states. In general, they can be represented in the following format:

$$\vec{\xi}' = \vec{f}(\vec{\xi}) \cdot \vec{u}, \tag{4.21}$$

where $\vec{\xi}$ is the state vector, $\vec{u}$ is the vector of inputs $(\vec{u} \equiv \mathbf{i})$, and $\vec{f}$ is a known matrix whose entries are nonlinear functions of the state. Our goal is to maintain a tracking control of the full state or of its part, which we denote as the output,

$$\mathbf{y} = C \cdot \xi. \tag{4.22}$$

Depending on the objectives, the output may be position or orientation of the dipole, but it can also contain velocities. We can also consider direct control of the forces and torques controls in the same general framework, because there exists a unique forward map from the forces and torques to the elements of the state vector, as described in eqn.1.1.

The system described by equation 4.21 is, in principle, state-linearizable, if the full state is measured precisely. This assumption is almost never entirely valid, but it leads to a useful approach nonetheless. Since $f(\cdot)$ is a matrix, we can represent it in a matrix form as $f(\xi) = \Omega$. If $\Omega$ is full rank, non-linearity in the states can be reversed and the inputs can be computed via

$$\vec{u} = \Omega^{-1} \cdot (-K\xi), \tag{4.23}$$

where $K$ is a positive-definite gain matrix designed to set the poles of the resultant linear system

$$\vec{\xi}' + K \cdot \vec{\xi} = \mathbf{0}. \tag{4.24}$$

If the state matrix $\Omega$ is singular, the above approach has to be modified. Singularity of $\Omega$ means, in general, that the number of inputs is insufficient to control the dynamics of the system. This may happen when there are not enough controllable field sources, but it can also occur when the sources are sufficiently coupled. The latter situation is quite common, but it occurs only at certain points and magnet orientations in the operating volume where the field lines from several sources coincide or lie sufficiently close to reduce the dimensionality of the control space. These points typically lie along the axes of symmetry of the coil system.

For an *overdetermined* system the above approach is best mended by making changes to the coil placement or by adding more coils. However, when that is impossible to do, we have to make the best of the situation by affecting the state dynamics to the extent that it

is controllable with the given inputs and avoiding the regions of the state-space where desired trajectory is unachievable. From the Pythagoras' theorem it follows that the tracking error is at its minimum when it is orthogonal to the space of the inputs. Therefore, by inverting the independent columns of the state matrix, (adjusting the independent field sources) we can minimize the error to the fullest extent possible. That is accomplish with the aid of *left pseudoinverse*, $\Omega^{L} \triangleq \left(\Omega^{T}\Omega\right)^{-1}\Omega$. It represents our best options at inverting the singular matrix $\Omega$. The inputs, then, take the form

$$\vec{u} = \Omega^{L} \cdot (-K\xi). \tag{4.25}$$

The other scenario, which we haven't yet considered, but which is usually the most common of the three, is that the system is *underdetermined*, so that several combinations of inputs achieve the desired result. This situation typically occurs on a subset of the operating region which contains all the desired trajectories of the dipole. Because the number of field sources (EM coils) is usually limited by the cost and by the geometric and power constraints of the problem, sufficient number is chosen so that all undesirable trajectories can be controlled or eliminated, and the placement of the coils is designed in such a way as to optimize the performance in a small subspace of the operating region where the magnet is most likely to remain or where it is best manipulated by the fields.

Since an underdetermined system has many solutions, a certain measure of cost is invented to evaluate and compare the quality of these solutions and to aid in choosing the most appropriate one. The cost function, in general, depends on the particular application and we will consider an example of such consideration in the next section; however, there

do exist general recipes regarding desirable performance criteria, the most common of which is minimization of the $\mathcal{L}^2$ norm of the input, $\vec{u}^{\mathrm{T}} \cdot \vec{u}$, which is typically proportional to the energy or power expenditure. (In the case considered below, it is a measure of static power consumption)

The solution that minimizes the square norm of the inputs is obtained with the aid of another "approximation" to the inverse of a state matrix, its *right pseudoinverse*, $\Omega^{\mathrm{R}} \triangleq \Omega^{\mathrm{T}}\left(\Omega \cdot \Omega^{\mathrm{T}}\right)^{-1}$, which is derived from the following identity: $(AA^{\mathrm{T}})(AA^{\mathrm{T}})^{-1} = I$. The right pseudoinverse, $A^{\mathrm{R}}$, provides the shortest possible solution $x^{+}$ to the equation

$$Ax = I \cdot y \Rightarrow Ax = A\left\{A^{\mathrm{T}}\left(AA^{\mathrm{T}}\right)^{-1}\right\} y \Rightarrow x^{+} \triangleq A^{\mathrm{T}}\left(AA^{\mathrm{T}}\right)^{-1} y, \tag{4.26}$$

because the difference of $x^{+}$ and any other solution $\hat{x}$ is in the nullspace of $A^{\mathrm{T}}A$, and so, it is also in the nullspace of $A$. Thus,

$$\left\|\hat{x}\right\|^2 = \left\|x^{+}\right\|^2 + \left\|\hat{x} - x^{+}\right\|^2 \geq \left\|x^{+}\right\|^2. \tag{4.27}$$

The inputs to the original problem are then computed as

$$\vec{u} = \Omega^{\mathrm{R}} \cdot (-K\xi). \tag{4.28}$$

If the inputs or the errors are weighted differently in the optimization process, a matrix of weights, $\mathbf{W}$, is introduced to reflect these differences. The weights are incorporated into the state equation via $\mathbf{W}\Omega\vec{u} = \mathbf{W}\vec{\xi}$ and the pseudoinverses are adjusted accordingly:

$$\begin{aligned} \Omega_w^{\mathrm{L}} &= \left(\Omega^{\mathrm{T}}\mathbf{W}^{\mathrm{T}}\mathbf{W}\Omega\right)^{-1}\Omega^{\mathrm{T}}\mathbf{W}^{\mathrm{T}}\mathbf{W} \\ \Omega_w^{\mathrm{R}} &= \Omega^{\mathrm{T}}\mathbf{W}^{\mathrm{T}}\left(\mathbf{W}\Omega\Omega^{\mathrm{T}}\mathbf{W}^{\mathrm{T}}\right)^{-1}\mathbf{W}. \end{aligned} \tag{4.29}$$

Then, the left pseudoinverse minimizes

$$\left\|\Omega\vec{u}-\vec{\xi}\right\|_w=\sqrt{\left[\mathbf{W}\cdot\left(\Omega\vec{u}-\vec{\xi}\right)\right]^{\mathrm{T}}\left[\mathbf{W}\cdot\left(\Omega\vec{u}-\vec{\xi}\right)\right]}=\sqrt{\sum_{i,j}w_{ij}\mathbf{e}_i\mathbf{e}_j} \tag{4.30}$$

and the right pseudoinverse minimizes $\left\|\vec{u}\right\|_w=\sqrt{\left(\mathbf{W}\vec{u}\right)^{\mathrm{T}}\left(\mathbf{W}\vec{u}\right)}=\sqrt{\sum_{i,j}w_{ij}u_iu_j}$. (4.31)

## 4.4 Power Optimization

A general cost function is formulated as the inverse of the Useful Work Coefficient for the system, which in turn, is defined as the ratio of the power output to the power input. Thus,

$$\mathscr{C}=\frac{P_{IN}}{P_{OUT}}. \tag{4.32}$$

$P_{IN}$ represents the cost of controlling magnetic field in the operating region, which is accomplished by setting and changing currents in the coils. We will consider a simple, resistive, coil system connected to a set of quasi-static power supplies. The "quasi-static" qualifier implies that the sources will operate mostly in a DC mode, but can be ramped up and down between their constant levels. This model is general enough to extend in a relatively straightforward manner to the superconducting systems, but sufficiently specific to capture the main aspects of the system's energetics.

### 4.4.1 Input Power

Consider a pair of inductive coils each connected to an independent voltage source and arranged in a transformer configuration, as shown below.

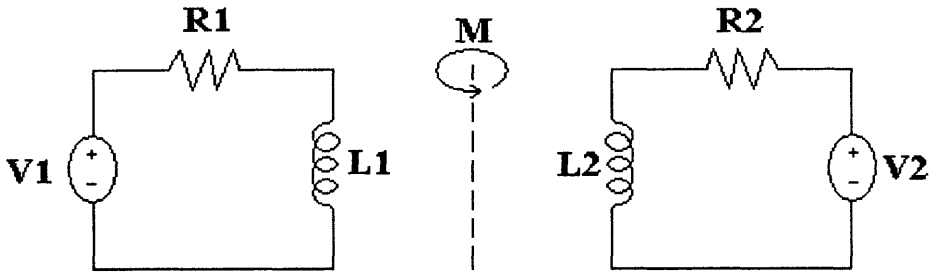


**Fig. 4.1 Solenoidal Coil Pair: RL circuit model**

For each individual coil, the circuit simplifies to an L-R configuration which includes the effects of the self-inductance, $L$, and the mutual inductance, $M$, as displayed in Fig. 4.2.

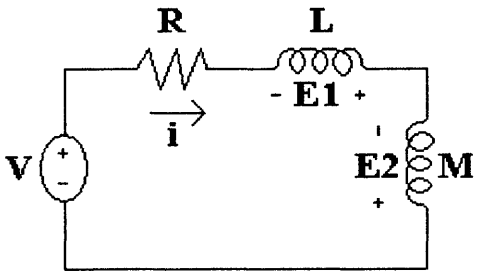


**Fig. 4.2 Single Coil: Transformer Model**

The inductive voltage drops are generated by changing currents in each of the coils, via

$$\mathcal{E}_1 = -L\frac{di_1}{dt} \quad \text{and} \quad \mathcal{E}_2 = -M\frac{di_2}{dt}. \tag{4.33}$$

Computing KVL around the loop, we obtain

$$\begin{aligned} v &= i_1 R + i_1' L + i_2' M_{12} \\ P_{IN1} &= i_1 v_1 = i_1^2 R + i_1 i_1' L + i_1 i_2' M_{12}. \end{aligned} \tag{4.34}$$

Likewise, for the second coil:

$$P_{IN2} = i_2 v_2 = i_2^{\,2} R + i_2 i_2' L + i_2 i_1' M_{21}. \tag{4.35}$$

The total power input for the pair is simply the sum of the two components. Due to the symmetry of the problem, the mutual inductances are equal: $M_{12} = M_{21}$. To simplify the computation, we can also consider the coils to be equivalent, so that $R_1 = R_2$ and $L_1 = L_2$. The total power is then equal to

$$P_{IN} = P_{IN1} + P_{IN2} = i_1 v_1 + i_2 v_2 = R\left(i_1^{\,2} + i_2^{\,2}\right) + \frac{L}{2}\frac{d}{dt}\left(i_1^{\,2} + i_2^{\,2}\right) + M\frac{d}{dt}(i_1 i_2). \tag{4.36}$$

Generalizing the results to a multiple-coil arrangement and introducing the resistive and inductive coefficient matrices,

$$\begin{aligned} \mathcal{R} &= \begin{bmatrix} R_1 & & & \\ & R_2 & & \\ & & R_3 & \\ & & & \ddots \end{bmatrix} = R \cdot \mathcal{I} \text{ (identity matrix)} \\ \mathcal{M} &= \begin{bmatrix} L_1 & M_{12} & M_{13} & \\ M_{21} & L_2 & M_{23} & \vdots \\ M_{31} & M_{32} & L_3 & \\ \cdots & & & \ddots \end{bmatrix} = \begin{bmatrix} L & M_{12} & M_{13} & \\ \bullet & L & M_{23} & \vdots \\ \bullet & \bullet & L & \\ \cdots & & & \ddots \end{bmatrix} = \mathcal{M}^{\mathrm{T}}, \end{aligned} \tag{4.37}$$

we obtain the total power input as a sum of bilinear products:

$$\begin{aligned} P_{IN} &= \sum_k R_k i_k^{\,2} + \frac{1}{2}\frac{d}{dt}\sum_k L_k i_k^{\,2} + \frac{d}{dt}\sum_{m \neq n} M_{m,n} i_m i_n \\ &= \mathbf{i}^{\mathrm{T}} \cdot \mathcal{R} \cdot \mathbf{i} + \mathbf{i}^{\mathrm{T}} \cdot \mathcal{M} \cdot \mathbf{i}' \end{aligned} \tag{4.38}$$

$$\boxed{P_{IN} = \langle \mathbf{i} | \mathbf{i} \rangle_{\mathcal{R}} + \langle \mathbf{i} | \mathbf{i}' \rangle_{\mathcal{M}}} \tag{4.39}$$

The first term in the sum represents resistive (DC) losses corresponding to the *static* power dissipation, whereas the second – represents inductive (AC) losses corresponding to *dynamic* power dissipation.

### 4.4.2 Output Power

The output power, $P_{OUT}$, represents the rate at which useful work is done on the system. In this context, the work is exerted in accelerating a dipole in a magnetic field. It depends both on the inputs (coil currents) and on the outputs (dipole position and orientation) of the system. By definition, the work equals the change in potential energy. Since the force on a dipole is equal to $\mathbf{F} = \nabla(\mathbf{p} \cdot \mathbf{B})$, its potential energy can be expressed as $\mathrm{U} = -\mathbf{p} \cdot \mathbf{B}$. The work $\delta W$ exerted in unit time $\delta t$ can be approximated as

$$\begin{aligned} &\delta W = -\delta \mathrm{U} = \mathbf{p} \cdot d\mathbf{B} + d\mathbf{p} \cdot \mathbf{B}, \text{where} \\ &d\mathbf{p} \triangleq \left(d\vec{\theta} \times \mathbf{p}\right) \text{and } \theta \triangleq \measuredangle\{\mathbf{p}, \mathbf{B}\}. \end{aligned} \tag{4.40}$$

Taking the limit as $\delta t \to 0$,

$$\begin{aligned} dW &= \mathbf{p} \cdot d\mathbf{B} + \left(d\vec{\theta} \times \mathbf{p}\right) \cdot \mathbf{B} \\ &= \mathbf{p} \cdot d\mathbf{B} + d\vec{\theta} \cdot (\mathbf{p} \times \mathbf{B}) \\ &= \mathbf{p} \cdot d\mathbf{B} + d\vec{\theta} \cdot \mathbf{T}, \end{aligned} \tag{4.41}$$

where $\mathbf{T}$ represents the torque exerted on the dipole to align its moment with the field. The instantaneous power output is then equal to

$$\begin{aligned} P_{OUT} &= \frac{dW}{dt} = \mathbf{p} \cdot \frac{d\mathbf{B}}{dt} + \mathbf{T} \cdot \frac{d\vec{\theta}}{dt} \\ \frac{d\mathbf{B}}{dt} &= \nabla \mathbf{B} \cdot \frac{d\mathbf{s}}{dt} + \frac{\partial \mathbf{B}}{\partial t} \end{aligned} \tag{4.42}$$

where **s** denotes the position of the dipole center of mass and so, the first summand represents the change in the field due to translation of the reference point (for *static* fields), while the second summand represent the change in the field due to the sources. (changing currents) Putting it all together,

$$\begin{aligned} P_{OUT} &= \underbrace{\mathbf{p}\cdot\nabla\mathbf{B}}_{\mathbf{F}}\cdot\underbrace{\frac{d\mathbf{s}}{dt}}_{\mathbf{v}} + \mathbf{p}\cdot\frac{\partial\mathbf{B}}{\partial t} + \mathbf{T}\cdot\underbrace{\frac{d\vec{\theta}}{dt}}_{\vec{\omega}} \\ &= \mathbf{F}\cdot\mathbf{v} + \mathbf{T}\cdot\vec{\omega} + \mathbf{p}\cdot\frac{\partial\mathbf{B}}{\partial t}. \end{aligned} \tag{4.43}$$

If the dipole is allowed to allow itself with the field (in the absence or total external torque),

$$\mathbf{T} = 0, \quad \mathbf{p} \,\|\, \mathbf{B} \Rightarrow \mathbf{p} = p\cdot\frac{\mathbf{B}}{B}, \tag{4.44}$$

then

$$\begin{aligned} P_{OUT} &= \frac{p}{B}\cdot(\mathbf{B}\cdot\nabla\mathbf{B})\cdot\mathbf{v} + \frac{p}{B}\cdot\left(\mathbf{B}\cdot\frac{\partial\mathbf{B}}{\partial t}\right) \\ &\propto \frac{p}{B}\cdot\left\{\mathbf{F}\cdot\mathbf{v} + \frac{d}{dt}\mathbf{B}^2\right\} \end{aligned} \tag{4.45}$$

The first term is proportional to the "effective" force exerted on the dipole, while the second term is proportional to the rate of change of the energy density stored in the magnetic field at point **s.**

$$\begin{aligned} &\mathbf{B}\cdot\nabla\mathbf{B} \propto \mathbf{F}, \quad \mathbf{B}\cdot\frac{\partial\mathbf{B}}{\partial t} \propto \frac{d}{dt}\left\{\frac{d\mathcal{U}}{dV}\right\}, \\ &\text{where } \mathcal{U} \propto \iiint_{\text{volume}} \mathbf{B}^2 dV. \end{aligned} \tag{4.46}$$

$\mathbf{B} = \mathcal{G}\cdot\mathbf{i}$, $\nabla\mathbf{B} = \mathcal{D}\cdot\mathbf{i}$, where $\mathcal{G}$ and $\mathcal{D}$ are functions of **s** and $\vec{\theta}$,

$$P_{OUT} = \frac{p}{\|\mathcal{G}\cdot\mathbf{i}\|}\left[\mathbf{i}^{\mathrm{T}}\underbrace{\mathcal{G}^{\mathrm{T}}\mathcal{D}}_{\mathcal{H}}\mathbf{i} + \mathbf{i}^{\mathrm{T}}\mathcal{G}^{\mathrm{T}}\mathcal{G}\mathbf{i}'\right]. \tag{4.47}$$

Translational cost function:

$$\mathscr{C}_{tr} = \frac{P_{IN}}{P_{OUT}} = \frac{\langle\mathbf{i}|\mathbf{i}\rangle_{\mathcal{R}} + \langle\mathbf{i}|\mathbf{i}'\rangle_{\mathcal{M}}}{\langle\mathbf{i}|\mathbf{i}\rangle_{\mathcal{H}} + \langle\mathbf{i}|\mathbf{i}'\rangle_{\mathcal{G}}}\cdot\frac{\sqrt{\langle\mathbf{i}|\mathbf{i}\rangle_{\mathcal{G}}}}{p} \tag{4.48}$$

Rotational cost function:

$$\mathscr{C}_{rot} = \frac{P_{IN}}{P_{OUT}} = \frac{\langle\mathbf{i}|\mathbf{i}\rangle_{\mathcal{R}} + \langle\mathbf{i}|\mathbf{i}'\rangle_{\mathcal{M}}}{(\mathbf{p}\times\mathcal{G}\mathbf{i})\cdot\vec{\omega}} = \frac{\langle\mathbf{i}|\mathbf{i}\rangle_{\mathcal{R}} + \langle\mathbf{i}|\mathbf{i}'\rangle_{\mathcal{M}}}{\underbrace{\cos\varphi}_{1\text{ if }\mathbf{T}=0}\cdot\sin\theta\cdot\dot{\theta}\cdot\langle\mathbf{i}|\mathbf{i}\rangle_{\mathcal{G}}}\cdot\frac{\sqrt{\langle\mathbf{i}|\mathbf{i}\rangle_{\mathcal{G}}}}{p} \tag{4.49}$$

# Chapter 5

# Conclusion

Non-contact manipulation of magnetized objects by means of electrically generated magnetic fields is a novel technology that has great potential benefits in a variety of application. Despite its promise and simplicity, the idea of magnetic manipulation has not been researched or explored in a centralized way and thus far it has led to relatively few commercial developments, especially in the area of large-gap systems. Part of the reason for the apparent lack of progress in the area has to do with the considerable technical difficulties inherent both in the construction of large electromagnets of sufficient strength and operating bandwidth and in the active control of the dynamics of manipulated objects. However, the idea is still to promising to abandon and recent advances in the superconducting magnetic technology have helped to renew the interest in the field.

The goal of this thesis is to provide a theoretical foundation that would elucidate and quantify the basic operating principles of magnetic manipulation technology and that

could serve as a convenient starting point for the new developments in the area. In the first chapter, several major implementations of the technology were surveyed and categorized according to their structure, size, and the intended mode of operation. A rather broad but virtually unexplored category of hypothetical devices has been chosen for detailed investigation and the main technological challenges inherent in their operation were identified and addressed in a general context.

The second chapter served to provide the quantitative background necessary for the design and analysis of the magnetic manipulation systems. Dynamics of a small permanent magnet was studied in the context of a point dipole model and equations of motion were developed for the interactions between the dipole and the ambient field. The issues of the relative importance of rotational and translational motions were investigated and theoretical prediction were formulated for some general operating scenarios.

The third chapter was devoted entirely to the computation of the magnetic field of a single solenoid. An accurate numerical representation of the field is of paramount importance to any successful dynamical analysis or control design of a magnetic system. Magnetic field was modeled for a range of simplifying assumptions of increasingly wider applicability and complexity. Both numerical and analytical expressions were derived to for use in the off-line and on-line field computations, and in the simulation of the dynamical behavior of the system. Although no physical field measurements were actually performed to verify the numerical predictions of the models, a previously

developed and experimentally calibrated finite element code was adopted for verification purposes. Within the scope of the operating assumptions, the various field representations were found to be in excellent agreement with the data. In particular, a very simple and accurate heuristic model of the fields was derived on the basis of the finite element code.

In the fifth chapter, the crucial equations describing the dynamics of the magnet and the structure of the fields were collected and expanded upon to provide a comprehensive quantitative description of the complete dynamical system. A general framework was laid down for analyzing the problem of the optimal selection and positioning of the magnetic field sources. Although solenoidal coils were used as the primary model for the sources, several general results were derived applicable to the coils of other geometries and to the stationary and movable permanent magnets. A simple MIMO controller was developed on the basis of feedback linearization technique and the concept of left- and right- pseudoinverses was introduced to deal with the over-constrained and under-constrained systems. Finally, a simple circuit model was developed for evaluating and optimizing the power efficiency of the entire system.

## 5.1 Future Directions

The present work was intended primarily as a starting point for subsequent analysis and new technical developments in the area of magnetic manipulation. Due to the rather large scope of the field and the generality of our approach, we decidedly refrained from focusing on any particular application or physical implementation of the system. In this

section, we point out some of the areas of investigation where we believe our efforts can be gainfully extended.

1. It would be instructive to perform a rigorous analysis of the optimal shapes and placements of electromagnetic coils in order to create magnetic field profiles appropriate for different dynamical tasks. For example, it is still unclear to what extent the fields can be shaped to independently manipulate several magnets at the same time. A thorough assessment of the fundamental limitations on field shaping, akin to Earnshaw's theorem, would be of great value in delineating the impossible and saving fruitless efforts.

2. Magnetic fields are generally inefficient for concentrating energy in a localized region of space. A careful study needs to be done to assess the maximum attainable efficiency for a general class of magnetic systems. Moreover, a consistent method for addressing these issues in the context of a particular application would be extremely useful both at the early stages of conceptual design and in the performance evaluation of a real system.

3. For any particular physical system, the fields should be carefully mapped out to insure that the models bear sufficient semblance to reality. Likewise, the forces and torques on a bar magnet should be measured experimentally to assess the validity and the limits of application of the point dipole model.

4. For a particular dynamical application, the repertoire of executable maneuvers should be cataloged and fundamental limitations on the performance of the system should be examined. A question of particular interest to us is to what extent the torques and forces on a bar magnet can be controlled independently and, in particular, what range of angles

between the field and the gradient can be achieved, for limited currents, at different points in the operating region.

# References:


[1] Knoepfel, H. E., *Magnetic Fields*, John Wiley & Sons, Inc: 2000

[2] Shadowitz, A., *The Electromagnetic Field*, McGraw-Hill: 1975

[3] Khalil, H. K., *Nonlinear Systems*, Prentice-Hall, Inc: 1996

[4] Slotine, J.-J. E., *et al*, *Applied Nonlinear Control*, Prentice-Hall, Inc: 1991

[5] Stengel, R.F., *Optimal Control and Estimation*, Dover Publications, Inc: 1994

[6] Strang, G., *Introduction to LinearAlgebra*, Wellesley-Cambridge Press: 1998

[7] Hamming, R.W., *Numerical Methods for Scientists and Engineers*, Dover: 1973

[8] Montgomery D.B., *et al*, "Magnetic Forces for Medical Applications," Journal of Applied Physics, v.40, n.3, 1969, pp.1039-1041

[9] Britcher, C.P., "Application of Magnetic Suspension Technology to Large Scale Facilities – progress, problems, and promises," AIAA, 1997, NAG1-1056